

1
2
3
4
5
6
7
8
9
10
11
12
13
14
15
16
17
18
19
20
21
22
23
24
25

Autonomous replication of the conjugative transposon Tn916

Laurel D. Wright and Alan D. Grossman*

Department of Biology

Massachusetts Institute of Technology

Cambridge, MA 02139

Short title: Autonomous replication of Tn916

*Corresponding author:
Department of Biology
Building 68-530
Massachusetts Institute of Technology
Cambridge, MA 02139
phone: 617-253-1515
email: adg@mit.edu

26 **Abstract**

27 Integrative and conjugative elements (ICEs), also known as conjugative transposons, are self-
28 transferable elements that are widely distributed among bacterial phyla and are important drivers
29 of horizontal gene transfer. Many ICEs carry genes that confer antibiotic resistances to their host
30 cells and are involved in the dissemination of these resistance genes. ICEs reside in host
31 chromosomes, but under certain conditions can excise to form a plasmid that is typically the
32 substrate for transfer. A few ICEs are known to undergo autonomous replication following
33 activation. However, it is not clear if autonomous replication is a general property of many
34 ICEs. We found that Tn916, the first conjugative transposon identified, replicates autonomously
35 via a rolling circle mechanism. Replication of Tn916 was dependent on the relaxase encoded by
36 *orf20* of Tn916. The origin of transfer of Tn916, *oriT(916)*, also functioned as an origin of
37 replication. Using immunoprecipitation and mass spectrometry, we found that the relaxase
38 (Orf20) and the two putative helicase processivity factors (Orf22 and Orf23) encoded by Tn916
39 likely interact in a complex and that the Tn916 relaxase contains a previously unidentified
40 conserved helix-turn-helix domain in its N-terminal region that is required for relaxase function
41 and replication. Lastly, we identified a functional single strand origin of replication (*ssO*) in
42 Tn916 that we predict primes second strand synthesis during rolling circle replication. Together
43 these results add to the emerging data that show that several ICEs replicate via a conserved,
44 rolling circle mechanism.

45

46

47 **Importance**

48 Integrative and conjugative elements (ICEs) drive horizontal gene transfer and the spread of
49 antibiotic resistances in bacteria. ICEs reside integrated in a host genome, but can excise to
50 create a plasmid that is the substrate for transfer to other cells. Here we show that Tn916, an ICE
51 with broad host range, undergoes autonomous rolling circle replication when in the plasmid
52 form. We found that the origin of transfer functions as a double-stranded origin of replication
53 and identified a single stranded origin of replication. It was long thought that ICEs do not
54 undergo autonomous replication. Our work adds to the evidence that ICEs replicate
55 autonomously as part of their normal lifecycle, and indicates that diverse ICEs use the same
56 replicative mechanism.

57

58

59

60 Introduction

61 Integrative and conjugative elements (ICEs), also called conjugative transposons, are mobile
62 genetic elements that encode proteins that mediate transfer of the element from the host cell
63 (donor) to a recipient by conjugation. ICEs often contain additional (cargo) genes that can
64 provide a selective advantage to the host cells (reviewed in 14, 40). Most ICEs have been
65 identified based on their cargo genes and the phenotypes conferred. For example, many ICEs
66 carry genes encoding antibiotic resistances. The horizontal dissemination of ICEs and their
67 associated cargo genes is a major driver of bacterial genome plasticity and evolution and the
68 spread of antibiotic resistances (e.g., 1, 56, 57, 67).

69 ICEs are typically found integrated in a host chromosome and are passively inherited by
70 vertical transmission via chromosomal replication and partitioning. When integrated, most ICE
71 genes are repressed. However, under certain conditions, or stochastically, ICE genes required
72 for excision and transfer are expressed and the ICE can excise from the genome. A site-specific
73 recombinase (integrase) catalyzes this excision and formation of a circular plasmid species that is
74 a substrate for conjugative transfer. All functional ICEs that use a type IV secretion system {i.e.,
75 ICEs outside of actinomyces (75)} encode an origin of transfer *oriT* and a cognate relaxase. The
76 relaxase nicks at a site in the *oriT* and becomes covalently attached to the 5' end of the DNA.
77 The nicked dsDNA is unwound and the relaxase attached to the ssDNA is transferred via a type
78 IV secretion system out of the donor and into a recipient cell to generate a transconjugant
79 (reviewed in 40, 82). In the transconjugant, the relaxase catalyzes re-circularization of the
80 ssDNA, releasing a ssDNA circle and a free relaxase.

81 The DNA processing steps accompanying conjugative transfer are similar to the steps
82 underlying rolling circle replication of some plasmids and phages (reviewed in 41). Plasmid

83 rolling circle replication initiates when a relaxase encoded by the plasmid nicks at the origin of
84 replication in the double stranded DNA (the double strand origin) and covalently attaches to the
85 5' end of the nicked strand. The nicked dsDNA is unwound and unidirectional replication
86 proceeds around the circle from the free 3'-end. The relaxase re-circularizes the nicked strand,
87 releasing a ssDNA circle. The ssDNA circle typically contains a single strand origin of
88 replication (*ssO*) that enables priming for DNA synthesis that converts the ssDNA to dsDNA.

89 ICEs that transfer ssDNA through a type IV secretion system were long thought to lack the
90 ability to replicate autonomously (12, 14, 82). ICEs can be maintained as integrated
91 chromosomal elements, and it appeared that ICEs could rely exclusively on vertical transmission
92 for inheritance. Furthermore, it is difficult to detect ICE replication because activation and
93 excision of most ICEs occur in a small fraction of donor cells.

94 However, there is compelling evidence that at least two ICEs undergo autonomous
95 replication. When de-repressed, *ICEBs1* from *Bacillus subtilis* undergoes autonomous rolling
96 circle replication (46, 76, 83). This replication initiates at the origin of transfer (*oriT*) after
97 nicking by the *ICEBs1*-encoded relaxase NickK (46). Processive unwinding of the nicked DNA is
98 dependent on the host translocase PcrA and the *ICEBs1*-encoded helicase processivity factor
99 Help (76). *ICEBs1* contains a single strand origin of replication (*ssO*) that enables second strand
100 synthesis (83). Recently, the ICE R391, a member of the SXT/R391 family of ICEs from *Vibrio*
101 *cholera* and *Providencia rettgeri*, was found to replicate autonomously in *Escherichia coli*, and
102 the relaxase and *oriT* of R391 are important for R391 replication (18). The copy number of
103 circularized SXT is also greater than the number of chromosomal sites from which it excised
104 (13), indicating that SXT undergoes autonomous replication and that replication is a conserved
105 feature of the SXT/R391 family of ICEs. R391 also encodes a conserved, functional plasmid

106 partitioning system (18), also consistent with autonomous replication and segregation. Other
107 ICEs and ICE-like elements may also be capable of autonomous, plasmid-like replication (16,
108 59, 77). However most ICEs activate and excise in a small fraction of cells (13, 19, 49, 51),
109 thereby hindering detection of replicating intermediates in population-based assays.

110 We were interested in determining if other ICEs found in Gram-positive bacteria are capable
111 of autonomous replication. We focused on Tn916 (Fig. 1A), the first conjugative transposon
112 identified (28, 29), and one of the most widely studied ICEs (62, 82). Tn916 and related elements
113 (e.g., Tn1545) contain a gene conferring resistance to tetracycline, exhibit a broad host range
114 (23), are found in many clinical isolates of *Enterococcus faecalis*, *Clostridium difficile*, and
115 *Streptococcus pneumoniae* (reviewed in 63), and can function in *B. subtilis* (22, 66). Unlike
116 many ICEs (e.g., ICEBs1, R391) that have a specific integration site, Tn916 can integrate into
117 multiple sites in a host genome, with a preference for AT-rich regions (52, 65).

118 We found that Tn916 is capable of autonomous replication in *B. subtilis*. Replication was
119 dependent on the relaxase encoded by Tn916 *orf20*. In addition, we found that the conjugative
120 origin of transfer of Tn916, *oriT(916)*, could also function as an origin of replication, and we
121 identified a functional *ssu* in Tn916. Our results demonstrate that Tn916 replicates autonomously
122 by rolling circle replication. These findings strengthen the model that many, and perhaps all,
123 functional ICEs undergo autonomous replication as part of their normal lifecycle.

124

125

126 **Materials and Methods**

127 **Media and growth conditions**

128 *Bacillus subtilis* cells were grown in LB medium or the MOPs-buffered S7₅₀ defined minimal
129 medium (37) as indicated. Cultures of cells containing pHP13-derived plasmids were grown for
130 imaging and ChIP-qPCR in medium containing 2.5 µg/ml chloramphenicol to select for the
131 plasmid as described (83). Cells containing *myc*-tagged *orf20* alleles were grown in medium
132 containing 50 µg/ml spectinomycin to maintain the single-cross-over integrations. Where
133 indicated, tetracycline (2.5 µg/ml) was added to Tn916-containing cells to increase gene
134 expression and excision (20). Antibiotics were otherwise used at the following concentrations:
135 kanamycin (5 µg/ml), chloramphenicol (5 µg/ml), spectinomycin (100 µg/ml), tetracycline (10
136 µg/ml), and a combination of erythromycin (0.5 µg/ml) and lincomycin (12.5 µg/ml) to select for
137 macrolide-lincosamide-streptogramin (*mls*) resistance.

138 **Strains**

139 *E. coli* strains used for plasmid construction were AG1111 (MC1061 F' *lacI*^q *lacZ*M15 Tn10)
140 (36) and TP611 (*thi thr leuB6 lacYI tonA21 supE44 hsdR hsdM recBC lop-11 cya-610 pcnB80*
141 *zad::Tn10*) (31).

142 *B. subtilis* strains were derived from JH642 (*pheA1 trpC2*) (58, 73) and are listed in Table 1.
143 Most strains were derived from JMA222, a derivative of JH642 that was cured of ICEBs1 (2).
144 The *ssb-mgfpmut2* fusion is expressed from the *rpsF* promoter and PrpsF-*ssb-mgfpmut2* was
145 inserted by double crossover at *lacA*, as described previously (5). Strains were constructed by
146 natural transformation (34).

147 *B. subtilis* strains containing Tn916. Tn916 host strain LDW173 was generated by natural
148 transformation of strain JMA222 with genomic DNA from strain BS49 (33) and selecting for

149 resistance to tetracycline as previously described (39). The Tn916 genomic integration site was
150 mapped by inverse PCR essentially as described (45). As in the parental strain (10), Tn916 is
151 integrated between chromosomal genes *yufK* and *yufL* at coordinate 3,209,748 (73). Tn916 is
152 oriented such that transcription of *orf24* and *int* of Tn916 is co-directional with that of *yufL*. This
153 insertion site is identical to one of the two Tn916 insertion sites found in strain BS49 (10). The
154 second Tn916 insertion in BS49 between *ykyB* and *ykuC* is not present in LDW173 and likely
155 was not transferred during transformation.

156 *orf20*. We constructed two mutations in the *orf20* (relaxase) gene. 1) Δ *orf20*-631 is a
157 markerless deletion that fuses the first 90 codons of *orf20* with the *orf20* stop codon, deleting the
158 intervening 306 codons and preserving *oriT(916)* (38). Two ~1 kb fragments containing DNA
159 flanking the deletion endpoints were PCR amplified and inserted into the BamHI and EcoRI sites
160 of pCAL1422 (a plasmid that contains *E. coli lacZ*) via isothermal assembly (30) as previously
161 described (76, 83). The resulting plasmid, pLW625, was integrated into the chromosome of
162 LDW173 (WT Tn916) via single-cross-over recombination. Transformants were screened for
163 loss of *lacZ*, indicating loss of the integrated plasmid, and PCR was used to identify a Δ *orf20*
164 clone. 2) The *orf20*-3UAA nonsense mutation replaces the third codon of *orf20*, GAA, with the
165 stop codon UAA. *orf20*-3UAA was also constructed by allelic replacement using essentially the
166 same strategy as for the Δ *orf20*-631 allele. Approximately 1 kb fragments containing DNA
167 flanking the point mutation site were PCR amplified using primers containing the G to T
168 mutation or its reverse complement. The two PCR products were inserted into the BamHI and
169 EcoRI sites of pCAL1422 via isothermal assembly, and the isothermal assembly product was
170 transformed directly into LDW173 (contains wild type Tn916) cells. Transformants were

171 screened for loss of *lacZ*, and mutants containing the G to T point mutation were identified by
172 sequencing. One such mutant (strain LDW853) was then used for experiments.

173 We fused various alleles of *orf20* to the LacI-repressible-IPTG-inducible promoter
174 Pspank(hy) and used these to test *orf20* function. Constructs included: Pspank(hy)-*orf20* (wild
175 type), present in strains LDW929 and LDW931; Pspank(hy)-*orf20* Δ *hth*-*myc* (missing the N-
176 terminal helix-turn-helix domain), present in strains LDW930 and LDW931. The wild type *orf20*
177 coding sequence begins at the CUG codon, whereas the *orf20* Δ *hth* coding sequence begins at the
178 annotated AUG start codon (see below). Both the *orf20* and *orf20* Δ *hth* expression constructs
179 include the 24 bases upstream of the presumed CUG start codon, including the putative ribosome
180 binding site ATTGGAGG. Both *orf20* and *orf20* Δ *hth* were PCR amplified from LDW173
181 genomic DNA, and the PCR fragments were inserted into the SphI and SacI sites of pCJ80 by
182 isothermal assembly. pCJ80 contains Pspank(hy) and the repressor *lacI*; an *mls* cassette marker;
183 and flanking homology for insertion by double-crossover into the chromosome at *lacA*. The
184 alleles were inserted into the chromosome by double-crossover, producing *lacA*::{ (Pspank(hy)-
185 *orf20*) *mls*} or *lacA*::{ (Pspank(hy)-*orf20* Δ *hth* *orf20*) *mls*}.

186 *orf20* and *orf20* Δ *hth* were tagged with three *myc* epitopes at the C-terminus, producing
187 *lacA*::Pspank(hy)-*orf20*-*myc* alleles, by single-crossover integration of a pCAL812-derived
188 plasmid as previously described (74). Briefly, ~1 kb of *orf20* encoding the C terminal end of the
189 protein that is common to both the wild type and *orf20* Δ *hth* alleles was PCR amplified and
190 inserted into the XhoI and EcoRI sites of pCAL812 by isothermal assembly, resulting in plasmid
191 pLW920. pLW920 was transformed into *lacA*::{Pspank(hy)-*orf20*} or *lacA*::{Pspank(hy)-
192 *orf20* Δ *hth*} by selecting for the spectinomycin resistance gene on pLW920.

193 *attITn916*. A copy of *attITn916* was inserted at *amyE* to make *amyE::{(attITn916) spc}* in
194 LDW737, a control strain for qPCR. *attITn916* was PCR amplified from DNA from LDW173
195 cells, which contain a small amount of excised *Tn916* circles. The PCR product was inserted via
196 isothermal assembly into the *EcoRI* and *HindIII* sites of pAS24, an *amyE* insertion vector that
197 contains a *spc* cassette.

198 Plasmids. Plasmids pLW805 and pLW859 are pUS19-based and contain *oriT(916)* and
199 *orf23*, *orf22* and *orf20* driven by Pspank. In pLW859, *orf20* is tagged with six histidine residues
200 at the 3' end. Pspank, *lacI* and an intervening multi-cloning site from pDR110 were inserted into
201 the *HindIII* and *EcoRI* sites in pUS19 to make pCAL799 (pDR110 is from D. Rudner, Harvard
202 Medical School) (4). *orf23* and *orf22* were PCR amplified from LDW173 and inserted into the
203 *NheI* and *SphI* sites in pCAL799 to make pLW521 (pUS19, Pspank-*orf23-orf22*, *lacI*). A
204 fragment encompassing *oriT(916)* (38) and *orf20* was PCR amplified from LDW173 and
205 inserted into the *SphI* site downstream of *orf22* in pLW521 to make pLW805 and pLW859. In
206 pLW859, the *his* tag was added to *orf20* with the downstream PCR primer.

207 We constructed pHP13 derivatives to test for SSO activity as previously described (83).
208 pLW868 (pHP13_{ss0916}) and pLW890 (pHP13_{ss0916R}) contain *ss0916* in the functional and
209 reverse orientation, respectively, relative to the direction of leading strand DNA synthesis of
210 pHP13 (32). We PCR amplified a 663 bp fragment from 89 bp upstream of the 3' end of *orf19*
211 through the first 458 bp of *orf18*, and inserted the fragment into the *BamHI* and *EcoRI* sites in
212 pHP13. *ssiA*, which forms a primosome assembly site, was PCR amplified from pHV1610-1
213 (11) to make pLW862 (pHP13_{ssiA}).

214 **Tn916 excision and replication**

215 We used qPCR to measure Tn916 excision and replication (Fig. 1B). Excision was measured
 216 using primers oLW542 (5'-GCAATGCGAT TAATACAACG ATAC) and oLW543 (5'-
 217 TCGAGCATTTC CATCATACAT TC) (Fig. 1B, primers a and d) to quantitate the vacant
 218 insertion site *attI*. *attI* amplification was normalized to a control chromosomal region in *mrpG*,
 219 which is 15 kb downstream of *attI*. *mrpG* was amplified with primers oLW544 (5'-
 220 CCTGCTTGGG ATTCTCTTTA TC) and oLW545 (5'-GTCATCTTGC ACACTTCTCT C).

221 The copy number of the Tn916 circle was measured with primer pair oLW526 (5'-
 222 AAACGTGAAG TATCTTCCTA CAG) and oLW527 (5'-TCGTCGTATC AAAGCTCATT C)
 223 (Fig. 1B, primers b and c) to quantitate the unique *attTn916* junction formed via site-specific
 224 recombination, and the average copy number of circular Tn916 per cell was calculated by
 225 normalizing *attTn916* amplification to *mrpG*. To determine if Tn916 was replicating, we
 226 determined the ratio of the copies of circular Tn916 to the copies of the excision site.

227 Copy numbers of *attTn916* and *attI* were determined by the standard curve method (15).
 228 Standard curves for *attTn916*, *attI* and control chromosome locus *mrpG* were generated from
 229 genomic DNA of LDW737, which contains one copy of each amplicon in the chromosome.
 230 LDW737 contains an ectopic copy of *attTn916* inserted at *amyE*. LDW737 does not contain
 231 Tn916 and therefore contains a copy of the unoccupied chromosome site *attI*. DNA for standard
 232 curves was prepared from stationary-phase LDW737 with an *oriC/terC* ratio of 1.3, verifying
 233 that *amyE::attTn916*, *attI* and *mrpG* were represented in ~1:1:1 ratios.

234 **Determination of copy number of an *oriT(916)* plasmid**

235 Copy number of plasmid pLW805 {*oriT(916)*, Pspank-*orf20-orf22-orf23*} was determined
 236 essentially as described (76). We used primers oLW128 (5'-ATGGAGAAGA TTCAGCCACT

237 GC) and oLW129 (5'-GCCATTATGG ATTCGTCAGA GG) that are specific to *spcE* in the
238 plasmid and normalized the amount of *spcE* to that of the chromosomal locus *mrpG*. Strain
239 LDW818 contains pLW805 inserted into Tn916 by single cross over and was used to represent a
240 plasmid copy number of one, and to generate standard curves to calculate plasmid copy number.

241 **Identification of the XRE-like helix-turn-helix domain**

242 We searched for conserved domains within *orf20* using the CUG start codon upstream of the
243 annotated AUG (Fig. 3A) using the NCBI Conserved Domain Database
244 (<http://www.ncbi.nlm.nih.gov/Structure/cdd/wrpsb.cgi>). The helix-turn-helix domain cd00093
245 was identified (E-value = 3.50e-10) along with the expected relaxase domain pfam02486. A
246 search for Orf20 homologues within ICEs using HMMER3::phmmer and the ICEberg database
247 yielded 101 hits, including relaxases containing the XRE-like helix-turn-helix domain (6). A
248 HMMER3::phmmer search of reference proteomes yielded additional relaxase homologues that
249 encoded the XRE-like helix-turn-helix domain and are present in a variety of sequenced Gram-
250 positive species (<http://www.ebi.ac.uk/Tools/hmmer/>).

251 **Orf20-His6 purification and mass spectrometry**

252 Orf20-His6 was purified from *B. subtilis* cells containing pLW859 (*oriT(916)*, Pspank-*orf23-*
253 *orf22-orf20-his6, spc*). Cells were grown to mid-exponential phase in LB medium containing 1
254 mM IPTG and 100 µg/ml spectinomycin. Cells from 250 ml of culture were pelleted, washed
255 with 1X phosphate-buffered saline (PBS), re-centrifuged and stored at -80°C. Pellets were
256 thawed on ice, and lysed in 25 ml binding buffer (300 mM NaCl, sodium phosphate buffer 50
257 mM, pH=7.4) containing 0.1 mg/ml lysozyme and the protease inhibitor 4-(2-aminoethyl)
258 benzenesulfonyl fluoride hydrochloride (AEBSF) at 1 mM at 37° C for 15 minutes. Lysates were

259 sonicated for 5 minutes total (0.3 sec. pulses, 15% output), followed by centrifugation to remove
260 insoluble material.

261 Lysates were pre-incubated with 0.5 ml TALON Superflow cobalt resin (GE Healthcare) on
262 a rotating platform for 1 hr at 4°C. Resin and lysate were loaded onto a Poly Prep column
263 (BioRad), and Orf20-His6 was purified according to GE Healthcare's protocol for batch, gravity-
264 flow purification under native conditions. Elution fractions were exchanged into buffer 20 mM
265 Hepes 150 mM KCl pH 7.5 using PD-10 desalting columns (GE Healthcare).

266 Purified protein was precipitated using trichloroacetic acid (TCA) and solubilized in 8 M
267 urea, 100 mM Tris, pH 8.5. Cysteines were reduced and alkylated using Tris 2-carboxyethyl
268 phosphine HCL (TCEP) and iodoacetamide respectively. The sample was then digested for four
269 hours at 37°C with endopeptidase Lys-C (Roche). The sample was then diluted to 2M Urea and
270 digested with trypsin (Promega). Peptides were identified using the LTQ XL Ion trap mass
271 spectrometer (Thermo Fisher) using MudPIT and SEQUEST software as previously described
272 (78). Tandem mass spectra were searched against a database of predicted ORFs from the genome
273 of *B. subtilis str. 168* (NCBI accession ASM904v1) and from *Tn916* (accession U09422.1),
274 including the predicted full length Orf20 sequence.

275 **Measurement of single strand origin activity**

276 We used live cell microscopy and ChIP-qPCR to analyze association of Ssb-GFP with
277 pHP13-derived plasmids containing DNA fragments with candidate *ssos* (83). ChIP-qPCR was
278 carried out as described (83). For imaging, cells were placed on a slice of agarose dissolved in
279 1X Spizizen's salts (2 g/l (NH₄)SO₄, 14 g/l K₂HPO₄, 6 g/l KH₂PO₄, 1 g/l Na₃ citrate-2H₂O, 0.2
280 g/l MgSO₄-7H₂O) (34) essentially as described (3). Images were acquired on a Nikon Ti-E
281 inverted microscope using a CoolSnap HQ camera (Photometrics). GFP fluorescence was

282 generated using a Nikon Intensilight mercury illuminator through Chroma filter set 49002.

283 Image processing was performed using ImageJ software.

284 **Results**

285 **Rationale**

286 Excision of Tn916 from a site in the chromosome yields two products (Fig. 1B): 1) the
287 vacated (empty) chromosomal attachment (integration) site, and 2) the circular plasmid form of
288 Tn916. We reasoned that if Tn916 replicates autonomously, then the copy number of the circular
289 form following excision would be greater than that of the chromosomal location that was vacated
290 upon excision. We used quantitative PCR (qPCR) to measure the amount of the empty
291 chromosomal integration site (called here *attI*) relative to a nearby gene (*mrpG*) and the amount
292 of the Tn916 circle relative to the amount of *attI* (Materials and Methods). We also reasoned
293 that if Tn916 replicates by rolling circle replication, then the Tn916 relaxase encoded by *orf20*
294 (Fig. 1A) would be required for replication.

295 **Excision of Tn916 from a site in the *B. subtilis* chromosome**

296 We measured the excision frequency of Tn916 from a chromosomal site in *B. subtilis* during
297 exponential growth and entry into stationary phase. *B. subtilis* strain LDW173 contains a copy of
298 Tn916 inserted between chromosomal genes *yufK* and *yufL* (*malK*) (Materials and Methods). We
299 used quantitative PCR to monitor excision from the *yufK-yufL* integration site, *attI*, and
300 normalized *attI* amplification to that of a nearby chromosomal locus, *mrpG*, that should be
301 unaffected by excision. We considered a strain without Tn916 to represent 100% excision (all
302 cells had *attI*) and we used this to generate standard curves to calculate excision frequencies.
303 (Materials and Methods).

304 There was a basal level of excision of Tn916 in cells growing exponentially in rich (LB)
305 medium (Fig. 2A). *B. subtilis* cells (strain LDW173) growing exponentially in LB medium were
306 diluted to a low density (OD600 ~0.05) in the absence or presence of tetracycline (see below). In
307 the absence of tetracycline we detected approximately 0.003 empty *attI* sites per *mrpG*, and
308 excision increased to approximately 0.01 *attI* sites per *mrpG* during exponential growth (Fig.
309 2A). After cells entered stationary phase, the amount of *attI* per *mrpG* appeared to decline (Fig.
310 2A). Based on these results, we infer that Tn916 had excised from *attI* in ~0.3-1% of cells
311 during exponential growth.

312 **Excision of Tn916 from a site in the *B. subtilis* chromosome is stimulated by tetracycline**

313 Excision of Tn916 requires the expression of *int* and *xis* (49) and these genes are downstream
314 of *tetM* (encoding tetracycline resistance) (Fig. 1A). The presence of tetracycline enhances
315 transcription of the genes needed for excision (20) and enhances excision of Tn916 from the
316 chromosome of *Enterococcus faecalis* (48). Conjugative transfer of Tn916 also increases in the
317 presence of tetracycline (20, 25, 48, 70), perhaps as a result of increased excision and/or
318 increased expression of the conjugation genes that become fused to the promoters driving *int* and
319 *xis* after excision and circularization. Interestingly, the amount of excision and conjugation and
320 the amount of stimulation by tetracycline is different for different insertion sites (48).

321 To determine the effects of tetracycline on excision of Tn916 from *attI* in *B. subtilis*,
322 exponentially growing cells were diluted to a low density into tetracycline (2.5 µg/ml), as
323 described above. Growth in the presence of tetracycline caused an increase in the amount of *attI*
324 per *mrpG* compared to cells grown in the absence of tetracycline (Fig. 2A), indicating that the
325 presence of tetracycline caused an increase in the excision frequency. This increase was most
326 apparent during entry into and during early stationary phase (Fig. 2A). There was a decline in

327 the amount of *attI* later in stationary phase. This decline could be indicative of death of cells
328 from which Tn916 had excised, thereby causing a decrease in the amount of *attI* (present in ~1-
329 3% of the cells) with relatively little overall affect on the amount of *mrpG* (present in almost all
330 cells). Alternatively, the decrease in *attI* could indicate that Tn916 reintegrated into *attI*.

331 **Autonomous replication of Tn916**

332 To measure the amount of the circular Tn916 after excision, we used a control that would
333 mimic 100% excision and a copy number of one Tn916 circle per chromosome. To generate this
334 control, we cloned the circular junction generated by excision of Tn916 from *attI* (*attI*Tn916,
335 Fig. 1B) and integrated a single copy of this DNA into the *B. subtilis* chromosome. We
336 considered a strain with *attI*Tn916 in single copy (and without any copies of Tn916; strain
337 LDW737) to represent 100% excision and a copy number of one. This strain was used in the
338 determination of the copy number of the circular form of Tn916 (Materials and Methods).

339 We used qPCR to measure the amount of the circular form of Tn916 relative to the
340 chromosomal locus *mrpG* from the same samples used to determine the amount of *attI* (above).
341 We found that, similar to the amount of *attI*, the amount of the circular form of Tn916 increased
342 during growth and reached a maximum as cells approached and entered stationary phase (Fig.
343 2B). The increase in copy number was most dramatic early in stationary phase where there was
344 a peak of ~0.2 copies of the circular form of Tn916 per copy of *mrpG* (Fig. 2B). This increase in
345 stationary was apparent following growth in the presence or absence of tetracycline, although the
346 copy number appeared to be ~2-fold higher in the presence of tetracycline (Fig. 2B).

347 We found that the copy number of the circular form of Tn916 was greater than that of the
348 vacated chromosomal site (*attI*) (Fig. 2C), indicating that there might be autonomous replication
349 of the excised form of Tn916. During exponential growth, this ratio was approximately 2-3 and

350 increased to ~10 circles per *attI* in stationary phase (Fig. 2C). These results indicate that the
351 copy number of the circle was greater than that of the empty chromosomal site and that the
352 excised Tn916 was most likely replicating autonomously. The increased copy number in
353 stationary phase compared to exponential growth is probably due to continued replication and
354 decreased cell growth.

355 **Increased copy number of the Tn916 circle was dependent on the relaxase encoded by**
356 **Tn916 *orf20***

357 Plasmids that use rolling circle replication require a plasmid-encoded relaxase (sometimes
358 called the initiator or replicase) that nicks DNA in the origin of replication (the double strand
359 origin or *dso*) to initiate unidirectional replication (41). Replicative relaxases are homologous to
360 conjugative relaxases (21, 26, 72). Some replicative relaxases can function in conjugation (47,
361 53, 69), and some conjugative relaxases can function in replication (46), thereby blurring the
362 distinction between replicative and conjugative relaxases.

363 We found that the conjugative relaxase of Tn916 (encoded by *orf20*) was needed for
364 autonomous replication of Tn916. The copy number of the Tn916 circle was significantly
365 reduced in the *orf20* mutant (Fig. 2B, C). There appeared to be a similar amount of excision in
366 the relaxase (Δ *orf20*) mutant as judged by the amount of *attI* compared to *mrpG* (Fig. 2A),
367 indicating that loss of the relaxase did not affect excision. However, the average copy number of
368 the circular form of Tn916 Δ *orf20* relative to the excision site was 0.39 ± 0.06 , and the copy
369 number remained relatively constant during the entire time course of the experiment (Fig. 2B,
370 C). This is considerably different from the ratio for the wild type Tn916 (*orf20*⁺). Together,
371 these results indicate that Tn916 normally undergoes autonomous rolling circle replication after
372 excision from the chromosome and the Tn916-encoded relaxase is required for this replication.

373 **The Tn916 origin of transfer *oriT* can function as an origin of replication**

374 If Tn916 uses its relaxase for rolling circle replication from *oriT*, then we expected that *oriT*
375 and *orf20* could function to support replication of a heterologous plasmid that is otherwise
376 missing an origin of replication. By analogy to ICEBs1 (76), we also expected that this
377 replication would also require the homologs of the ICEBs1 helicase processivity factor *HelP* that
378 are encoded by Tn916 *orf22* and *orf23*.

379 We found that the Tn916 origin of transfer *oriT(916)* could function as an origin of
380 replication. We cloned *oriT(916)* into a plasmid that is otherwise incapable of autonomous
381 replication in *B. subtilis*. The parent plasmid, pUS19 (4), contains a pUC origin that is not
382 functional in *B. subtilis* but is functional in *E. coli*. pUS19 also contains *spcE*, conferring
383 resistance to spectinomycin in *B. subtilis*. In addition to *oriT(916)*, we cloned the genes *orf20*
384 (relaxase), and *orf22* and *orf23* (*helP* homologues) from Tn916 to generate plasmid pLW805. In
385 this plasmid, transcription of *orf20*, *orf22*, and *orf23* is controlled by the LacI-repressible-IPTG-
386 inducible promoter Pspank (Pspank-*orf23-orf22-orf20*), making expression of these genes
387 dependent on IPTG.

388 We transformed cells lacking Tn916 with pLW805 {*oriT(916)*, Pspank-*orf23-orf22-orf20*}
389 DNA (that had been isolated from *E. coli*) and selected for spectinomycin-resistant
390 transformants. Transformants were obtained in the presence of IPTG (enabling expression of
391 *orf20*, *orf22*, and *orf23*), but no transformants were obtained in the absence of IPTG. These
392 results indicate that *oriT* was capable of supporting replication and that replication was likely
393 dependent on expression of the relaxase and perhaps the *helP* homologues. The plasmid copy
394 number was approximately 4 ± 1 per cell as determined by qPCR of *spcE* plasmid DNA relative
395 to the chromosomal locus *mrpG*.

396 The *oriT(916)* plasmid (pLW805) was unstable, even when cells were grown in IPTG and
397 spectinomycin. The fraction of plasmid-containing cells was determined by counting colony
398 forming units (CFUs) on LB agar plates containing IPTG and spectinomycin or on LB agar
399 without additives. After 7-8 generations of exponential growth in liquid LB medium with IPTG
400 and spectinomycin, approximately $17 \pm 6\%$ of cells were able to form colonies on LB plates with
401 IPTG and spectinomycin (the total number of cells was determined by CFUs on LB plates with
402 neither spectinomycin nor IPTG), indicating that the plasmid had been lost from ~83% of the
403 cells growing in culture. This is not surprising for a plasmid that has a relatively low copy
404 number, replicates by rolling circle replication, lacks a single strand origin of replication, and
405 lacks partitioning functions.

406 The *oriT(916)* plasmid (pLW805) was even more unstable when cells were grown non-
407 selectively and in the absence of IPTG (causing decreased expression of *orf20*, *orf22*, and *orf23*).
408 Plasmid-containing cells were transferred to medium lacking IPTG and spectinomycin, and after
409 7-8 generations of exponential growth without inducer or selection, only 0.2% of cells were
410 resistant to spectinomycin, indicating that the *oriT* plasmid was lost in >99.5% of cells. These
411 results indicate that expression of the relaxase and perhaps the predicted helicase processivity
412 factors was needed for plasmid propagation. Based on what is known about rolling circle
413 replication and the functions of the relaxase and helicase processivity factors (e.g., 76), and the
414 finding that the relaxase was needed for replication of Tn916 (Fig. 2C), we conclude that
415 replication from *oriT(916)* was dependent on the relaxase (*orf20*) and probably at least one of the
416 HelP homologues (*orf22*, *orf23*). Results below indicate that the relaxase and both HelP
417 homologues are associated with the plasmid replicating from *oriT(916)*.

418 Analysis of Orf20 reveals a conserved N-terminal helix-turn-helix domain

419 Tn916 *orf20* (relaxase) is annotated to start with an AUG codon (Fig. 3A, B) (64). We
420 noticed that *orf20* lacks an obvious ribosome binding site (RBS) upstream of the putative start
421 codon. However, there is a potential ribosome binding site and CUG start codon upstream of the
422 annotated AUG start (Fig. 3B). The predicted protein generated using this CUG start includes a
423 helix-turn-helix (HTH) domain that is found in the xenobiotic response element (XRE)-like
424 family of DNA-binding proteins (e.g., the repressor Xre of the *B. subtilis* defective phage PBSX;
425 lambda cI and Cro) (NCBI accession cd00093) (50, 55, 80, 81).

426 The XRE-like helix-turn-helix domain is conserved in many homologues of the *orf20*-
427 encoded relaxase (see Materials and Methods), including the relaxases of Tn916-related elements
428 present in multi-drug-resistant *C. difficile* strain 630 (CTn7) and in pathogenic strains of *S.*
429 *pneumonia* (Tn5253), and relaxases present in putative mobile elements from several Gram-
430 positive species (35, 63, 67) (Fig. 4). We suspect that some *orf20* homologues were misannotated
431 based on the initial annotation of Tn916 *orf20*. In the reference genomes (e.g., relaxase *orf26* in
432 CTnI; Fig. 4) there are sequences encoding a potential HTH motif in or immediately upstream of
433 the annotated start codon (8, 9, 67), consistent with the notion that the actual relaxase is larger
434 than that originally annotated. Other *orf20* homologues, including the relaxase Nick from
435 ICEBsI, do not contain an XRE-like helix-turn-helix domain.

436 We postulated that the Tn916 relaxase was larger than previously predicted and contained a
437 conserved helix-turn-helix domain. To test this, we analyzed peptide fragments from purified
438 relaxase. We fused a hexahistidine tag to the C-terminus of the relaxase (Orf20-his) in the
439 *oriT(916)* plasmid (generating pLW859). Like the parent plasmid, the plasmid with *orf20-his*
440 was capable of autonomous replication in *B. subtilis* (strain LDW879), indicating that Orf20-his

441 was functional. We purified Orf20-his from *B. subtilis* and analyzed the protein by mass
442 spectrometry. We identified peptides from both the N-terminal helix-turn-helix and C-terminal
443 relaxase regions (Fig. 3A, Table 2). These results indicate that cells produce Orf20 starting with
444 the CUG codon and containing the helix-turn-helix region.

445 To verify that the helix-turn-helix region was part of the relaxase, we made a nonsense
446 mutation in this region of *orf20*. We mutated the third codon downstream of the presumed CUG
447 start codon to a stop codon (*orf20-3UAA*) (Fig. 3B). Like the *orf20* deletion, the *orf20-3UAA*
448 nonsense mutation abolished replication of Tn916 (Table 3). Replication was restored to both
449 Tn916 Δ *orf20* and Tn916*orf20-3UAA* when full-length *orf20* (*orf20-myc*), starting with the CUG
450 codon and containing a C terminal *myc* tag, was expressed from Pspank(hy) (Table 3).
451 Abrogation of relaxase function with the *orf20-3UAA* mutation indicates that the annotated AUG
452 start codon in Tn916 (Fig. 3B) does not initiate translation of a functional relaxase and that the
453 start codon is most likely upstream of the position of the nonsense mutation.

454 We also overexpressed the previously annotated *orf20*, missing the helix-turn-helix domain
455 (*orf20 Δ hth-myc*), from Pspank(hy). The Pspank(hy)-*orf20 Δ hth-myc* allele was unable to
456 complement the replication defects of relaxase-deficient Tn916 (Table 3). The simplest
457 interpretation of these results is that the helix-turn-helix domain of Orf20 is required for
458 replication.

459 Based on results above, we conclude that the actual *orf20* open reading frame contains the
460 helix-turn-helix motif found in many XRE-like proteins. Furthermore, the open reading frame
461 most likely begins at the CUG codon that is preceded by a potential ribosome binding site (Fig.
462 3). It seems reasonable to retain the name *orf20* for the Tn916 gene encoding the conjugative
463 (and replicative) relaxase, recognizing that in some of the literature, this refers to the shorter

464 open reading frame, but in many cases, the exact coding sequence is not so important for the
465 genetic analyses. It would also be reasonable to change the name of the Tn916 gene for the
466 relaxase, perhaps calling it *nicK*, adopting the name used for the ICEBs1-encoded relaxase.
467 Here, we continue to refer to the full length relaxase gene as *orf20*.

468 **Association of HelP homologues Orf23 and Orf22 with relaxase Orf20-his**

469 The plasmid replicating from *oriT(916)* with *orf20-his* (pLW859) also contained *orf23* and
470 *orf22* from Tn916, the homologues of ICEBs1 *helP*. Mass spectrometry of affinity-purified
471 Orf20-his identified peptides from both Orf23 and Orf22 (Table 2). Co-purification of the HelP
472 homologues with functional relaxase indicates that the HelPs are part of the relaxosome and are
473 likely important for replication from *oriT*. These data are consistent with the model that Tn916
474 replicates by a rolling circle mechanism and uses helicase processivity factors to facilitate
475 unwinding of the DNA strands after relaxase nicking, analogous to autonomous replication of
476 ICEBs1.

477 **Identification of a single strand origin in Tn916**

478 Because Tn916 replicates by rolling circle replication, we expected it would have a single
479 strand origin of replication. Rolling circle replicating plasmids and phages contain an *sso* or
480 encode a primase that enables conversion of ssDNA to dsDNA (42-44, 79). ICEBs1 has a single
481 strand origin that enables second strand synthesis (83).

482 We tested parts of Tn916 for *sso* activity using a plasmid-based assay. pHP13 is a rolling
483 circle replicating plasmid that lacks an *sso* and accumulates ssDNA (7). In cells expressing a
484 fusion of the host single stranded DNA binding protein to GFP (Ssb-GFP), accumulation of
485 ssDNA can be visualized as large fluorescent foci of Ssb-GFP in most pHP13-containing cells
486 (Fig. 5A and B, strains CMJ118 without plasmid and CMJ129 with pHP13). We previously

487 found that when pHP13 contains *ssol* from *ICEBs1*, there is a reduction in the size and intensity
488 of Ssb-GFP foci (83). Similarly, *ssiA* from pAM β , which is a primosome assembly site (11),
489 reduces pHP13 ssDNA (Fig 5C, pLW862, strain LDW872), showing that this fluorescent-
490 microscopy based assay, in conjunction with the pHP13 vector can be used to rapidly screen
491 single strand origins of multiple types (RNAP- vs. primase-dependent).

492 Most *sso*'s in RCR plasmids are found in intergenic regions and are orientation-specific (42).
493 Therefore, we cloned several intergenic regions from *Tn916* into pHP13 and screened for a
494 reduction in ssDNA accumulation as visualized by a reduction in the size of Ssb-GFP foci. One
495 of the regions we screened, encompassing the intergenic region between *orf19* and *orf18* (Fig.
496 1A), reduced ssDNA (pLW858, strain LDW878) (Fig. 5D). In addition, we found that the Sso
497 activity of the '*orf19-orf18*' region was orientation-specific. That is, the fragment cloned in the
498 opposite orientation into pHP13 (pLW890, strain LDW894) did not reduce the size or intensity
499 of Ssb-GFP foci (Fig. 5E). The predicted secondary structure of the sequence in this region did
500 not appear to resemble any of the three common types of *sso*'s, *sso_A*, *sso_U*, or *sso_T* (42) whereas
501 *ssol* from *ICEBs1* resembles that from pTA1060 (83) and belongs to the *sso_T* family.

502 We quantified Sso activity of the '*orf19-orf18*' fragment (referred to as *sso916*) by
503 immunoprecipitating Ssb-GFP and determining the amount of plasmid DNA bound to Ssb
504 (ssDNA) using qPCR (Fig.6). *sso916* (present in pLW858) reduced the amount of Ssb-bound
505 plasmid DNA ~30-fold, similar to *ssol* from *ICEBs1* (83). In contrast, in cells containing
506 pLW890 (pHP13 with *sso916R*, *sso916* in the opposite orientation), the amount of plasmid DNA
507 bound to Ssb-GFP was similar to that of the parent plasmid (pHP13) without an *sso* (Fig. 6). The
508 differences in the amount of Ssb-GFP bound to each of the plasmids was not due to differences
509 in plasmid copy number. The copy number of pLW858 (pHP13 with *sso916*) was approximately

510 the same as that of pHP13, and that of pLW890 (pHP13 with *sso916R*) was approximately 1.4-
511 fold that of pHP13.

512 We found that *sso916* is conserved in other Tn*916*-like ICEs. We searched for sequences
513 similar to the 116 bp intergenic region that contains *sso916* and found that 15 additional ICEs
514 contained a region with 94-100% sequence identity (Table 4). The conjugation genes from all of
515 these ICEs are highly similar ($\geq 80\%$ identity) to those in Tn*916*, but each contains accessory
516 (cargo) genes different from those in Tn*916*. Based on these results, we conclude that *sso916* is a
517 functional single strand origin of replication in Tn*916* that has been conserved during genetic
518 diversification of Tn*916*-like elements.

519

520

521 **Discussion**

522 **Tn*916* replicates autonomously**

523 We found that the broad-host range conjugative transposon Tn*916* undergoes autonomous
524 rolling-circle replication. The excised circular form of Tn*916* is multi-copy, and replication is
525 dependent on the relaxase encoded by *orf20*. The Tn*916* origin of transfer *oriT(916)* supports
526 replication of a plasmid that is otherwise incapable of replication in *B. subtilis*. Replication
527 appears to be dependent on the relaxase and at least one and perhaps both of the helicase
528 processivity factor homologues Orf23 and Orf22. Co-purification of the relaxase and both Help
529 homologues indicates that both of the Help homologues are likely functioning in DNA
530 unwinding. We do not know if one or the other or both are required, nor if they are redundant.
531 Lastly, Tn*916* contains a functional *sso*, *sso916*. Our results support a model in which relaxase
532 Orf20 initiates rolling circle replication from *oriT(916)* and the Help homologues facilitate

533 processive unwinding of the nicked strand, analogous to the role of the relaxase and Help in
534 ICEBs1 (46, 76). After recircularization of the unwound strand, Sso activity would be used to
535 initiate priming of lagging strand DNA synthesis.

536 Tn916 was thought to be incapable of autonomous replication. Previous studies may have
537 failed to detect replicating Tn916 because, like many ICEs, Tn916 excises in a small fraction of
538 host cells (19, 49). The circular form of Tn916 was detected using Southern blotting when *xis*
539 and *int* were overexpressed (49). The ratio of Tn916 circles per excision event was reported to be
540 1.8 Tn916 circles per excision site. We observed a similar ratio when nutrients were non-limiting
541 (~1-3 circles per excision sites during exponential growth, Fig. 2C).

542 Tn916 excision and copy number peaked during early stationary phase. Likewise, maximal
543 excision of Tn916 in *E. faecalis* and *Listeria monocytogenes* occurs during late exponential
544 phase (19), consistent with the notion that activation of Tn916 is dependent, in part, on cell
545 growth phase. Other ICEs also have growth-phase-dependent excision due to nutrient limitation,
546 in response to cell-cell signaling, or both (2, 17, 59, 60, 68).

547 **Identification of an N-terminal helix-turn-helix domain in the Tn916-encoded relaxase**

548 We identified a conserved helix-turn-helix domain in the N-terminal region of the relaxase
549 Orf20. This domain is conserved in many relaxase homologues and our results indicate that this
550 region is essential for relaxase function.

551 A purified form of Orf20 from Tn916 nicks *oriT(916)* non-specifically *in vitro*, and co-
552 incubation with the recombinase Int then generated strand- and sequence-specific nicking (64).
553 However, because *orf20* was misannotated, Orf20 used in these experiments was purified
554 without the N-terminal helix-turn-helix domain. Our results indicate that Orf20 contains an N-
555 terminal helix-turn-helix domain. Because *oriT(916)* functions as an origin of replication in the

556 absence of *int*, we suggest that Int is not involved in nicking *oriT(916)* and that the helix-turn-
557 helix domain in Orf20 likely facilitates recognition of *oriT(916)*.

558 A class of conjugative relaxases from plasmids has recently been described that contain an
559 N-terminal helix-turn-helix motif (27), although the domain is not a member of the XRE-like
560 family present in Orf20. Mutation of a highly conserved glutamate residue in the helix-turn-helix
561 domain of representative relaxase TraX prevented relaxase binding to *oriT* (27), consistent with
562 the model that the N-terminal helix-turn-helix domain in Orf20 is needed for proper recognition
563 and nicking of *oriT(916)*.

564 **Replication and maintenance**

565 Replication of ICEBs1 and R391 is required for maintenance of the elements in dividing host
566 cells (18, 46), and studies with other ICEs found that the relaxase is required for stability of the
567 cognate ICE (e.g., 59). However, we did not observe a significant loss of a Tn916 Δ *orf20* mutant
568 (missing the relaxase). This apparent stability could indicate that the circular form of Tn916
569 might cause growth arrest or possibly cell death. No genes in Tn916 have been identified that
570 cause such a phenotype, but there are several genes with unknown function. We also observed a
571 decrease in signal of *attI* during stationary phase. This is consistent with Tn916 reintegration
572 into *attI* or death of cells in which Tn916 has excised. We do not favor the first hypothesis
573 because Tn916 can integrate into multiple sites (52, 54, 61), and we have observed that Tn916
574 does not have a preference for reintegration into *attI* in transconjugants (Wright and Grossman,
575 unpublished results).

576 Some ICEs are known to cause growth arrest and/or cell death. For example, when activated,
577 ICE*clc*, an ICE active in *Pseudomonas* species, can inhibit host cell growth (~50% of activated
578 cells stop dividing) and cause cell lysis (24, 60). Despite the damage incurred by host cells, 75%

579 of donors with excised ICE*clc* that contact a recipient cell successfully transfer the element (24).
580 Single-cell microscopy studies, such as those conducted on ICE*clc*, are required to assess the
581 affect of Tn*916* induction on host cell fate.

582 **Autonomous replication of integrative and conjugative elements is conserved**

583 Growing evidence indicates that several ICEs replicate autonomously by a common
584 mechanism. ICE*Bs1* and Tn*916* both replicate by a rolling circle mechanism using similar
585 machinery. However, ICE*Bs1* and Tn*916* are very different elements, with different regulatory
586 mechanisms, different modes of integration, and different cargo genes. The ICE R391 also
587 replicates autonomously in Gram-negative *E. coli*, and its relaxase and *oriT* are important for
588 replication, indicating that R391 likely also uses rolling circle replication. Since all functional
589 ICEs that use a type IV secretion system have an origin of transfer and a cognate relaxase, the
590 accumulating findings support the notion that many, and perhaps all, ICEs are capable of
591 autonomous rolling circle replication.

592

593

594 **Acknowledgements**

595 We thank C. Lee and C. Johnson for helpful discussions, M. Laub and S. Bell for comments
596 on the manuscript, M. Avello and C. Lee for mapping the Tn*916* insertion site in LDW173, and
597 D. Kern and I. Cheeseman for assistance with the mass spectrometry.

598 Research reported here is based upon work supported, in part, by the National Institute of
599 General Medical Sciences of the National Institutes of Health under award number
600 R01GM050895 to ADG. LDW was also supported, in part, but NIGMS pre-doctoral training
601 grant T32GM007287. Any opinions, findings, and conclusions or recommendations expressed in

602 this report are those of the authors and do not necessarily reflect the views of the National
 603 Institutes of Health.

604

605

606 **References**

607

- 608 1. **Amita, S. R. Chowdhury, M. Thungapathra, T. Ramamurthy, G. B. Nair, and A.**
 609 **Ghosh.** 2003. Class I integrons and SXT elements in El Tor strains isolated before and
 610 after 1992 *Vibrio cholerae* O139 outbreak, Calcutta, India. *Emerg Infect Dis* **9**:500-502.
- 611 2. **Auchtung, J. M., C. A. Lee, R. E. Monson, A. P. Lehman, and A. D. Grossman.** 2005.
 612 Regulation of a *Bacillus subtilis* mobile genetic element by intercellular signaling and the
 613 global DNA damage response. *Proc Natl Acad Sci U S A* **102**:12554-12559.
- 614 3. **Babic, A., M. B. Berkmen, C. A. Lee, and A. D. Grossman.** 2011. Efficient gene transfer
 615 in bacterial cell chains. *mBio* **2**:00027-00011.
- 616 4. **Benson, A. K., and W. G. Haldenwang.** 1993. Regulation of sigma-B levels and activity
 617 in *Bacillus subtilis*. *J Bacteriol* **175**:2347-2356.
- 618 5. **Berkmen, M. B., and A. D. Grossman.** 2006. Spatial and temporal organization of the
 619 *Bacillus subtilis* replication cycle. *Mol Microbiol* **62**:57-71.
- 620 6. **Bi, D., Z. Xu, E. M. Harrison, C. Tai, Y. Wei, X. He, S. Jia, Z. Deng, K. Rajakumar,**
 621 **and H. Y. Ou.** 2012. ICEberg: a web-based resource for integrative and conjugative
 622 elements found in Bacteria. *Nucleic Acids Res* **40**:D621-626.
- 623 7. **Bron, S., W. Meijer, S. Holsappel, and P. Haima.** 1991. Plasmid instability and
 624 molecular cloning in *Bacillus subtilis*. *Res Microbiol* **142**:875-883.
- 625 8. **Brouwer, M. S., A. P. Roberts, P. Mullany, and E. Allan.** 2012. In silico analysis of
 626 sequenced strains of *Clostridium difficile* reveals a related set of conjugative transposons
 627 carrying a variety of accessory genes. *Mob Genet Elements* **2**:8-12.
- 628 9. **Brouwer, M. S., P. J. Warburton, A. P. Roberts, P. Mullany, and E. Allan.** 2011.
 629 Genetic organisation, mobility and predicted functions of genes on integrated, mobile
 630 genetic elements in sequenced strains of *Clostridium difficile*. *PLoS One* **6**:e23014.
- 631 10. **Browne, H. P., S. Y. Anvar, J. Frank, T. D. Lawley, A. P. Roberts, and W. K. Smits.**
 632 2015. Complete genome sequence of BS49 and draft genome sequence of BS34A, *Bacillus*
 633 *subtilis* strains carrying Tn916. *FEMS Microbiol Lett* **362**:1-4.
- 634 11. **Bruand, C., S. D. Ehrlich, and L. Janniere.** 1995. Primosome assembly site in *Bacillus*
 635 *subtilis*. *EMBO J* **14**:2642-2650.
- 636 12. **Burrus, V., G. Pavlovic, B. Decaris, and G. Guedon.** 2002. Conjugative transposons: the
 637 tip of the iceberg. *Mol Microbiol* **46**:601-610.
- 638 13. **Burrus, V., and M. K. Waldor.** 2003. Control of SXT integration and excision. *J*
 639 *Bacteriol* **185**:5045-5054.
- 640 14. **Burrus, V., and M. K. Waldor.** 2004. Shaping bacterial genomes with integrative and
 641 conjugative elements. *Res Microbiol* **155**:376-386.
- 642 15. **Bustin, S. A., and T. Nolan.** 2004. Data analysis and interpretation, p. 439-492. *In* S. A.
 643 Bustin (ed.), *A-Z of quantitative PCR*. <http://www.fivephoton.com>.

- 644 16. **Carraro, N., V. Libante, C. Morel, F. Charron-Bourgoin, P. Leblond, and G. Guedon.**
645 2016. Plasmid-like replication of a minimal Streptococcal Integrative and Conjugative
646 Element. *Microbiology* **162**:622-632.
- 647 17. **Carraro, N., V. Libante, C. Morel, B. Decaris, F. Charron-Bourgoin, P. Leblond, and**
648 **G. Guedon.** 2011. Differential regulation of two closely related integrative and conjugative
649 elements from *Streptococcus thermophilus*. *BMC Microbiol* **11**:238.
- 650 18. **Carraro, N., D. Poulin, and V. Burrus.** 2015. Replication and Active Partition of
651 Integrative and Conjugative Elements (ICEs) of the SXT/R391 Family: The Line between
652 ICEs and Conjugative Plasmids Is Getting Thinner. *PLoS Genet* **11**:e1005298.
- 653 19. **Celli, J., C. Poyart, and P. Trieu-Cuot.** 1997. Use of an excision reporter plasmid to
654 study the intracellular mobility of the conjugative transposon Tn916 in gram-positive
655 bacteria. *Microbiology* **143 (Pt 4)**:1253-1261.
- 656 20. **Celli, J., and P. Trieu-Cuot.** 1998. Circularization of Tn916 is required for expression of
657 the transposon-encoded transfer functions: characterization of long tetracycline-inducible
658 transcripts reading through the attachment site. *Mol Microbiol* **28**:103-117.
- 659 21. **Chandler, M., F. De La Cruz, F. Dyda, A. B. Hickman, G. Moncalian, and B. Ton-**
660 **Hoang.** 2013. Breaking and joining single-stranded DNA: the HUH endonuclease
661 superfamily. *Nat Rev Microbiol* **11**:525-538.
- 662 22. **Christie, P. J., R. Z. Korman, S. A. Zahler, J. C. Adsit, and G. M. Dunny.** 1987. Two
663 conjugation systems associated with *Streptococcus faecalis* plasmid pCF10: identification
664 of a conjugative transposon that transfers between *S. faecalis* and *Bacillus subtilis*. *J*
665 *Bacteriol* **169**:2529-2536.
- 666 23. **Clewell, D. B., and S. E. Flannagan.** 1993. The Conjugative Transposons of Gram-
667 Positive Bacteria, p. 369-393. *In* D. B. Clewell (ed.), *Bacterial Conjugation*. Plenum Press,
668 New York, NY.
- 669 24. **Delavat, F., S. Mitri, S. Pelet, and J. R. Van Der Meer.** 2016. Highly variable individual
670 donor cell fates characterize robust horizontal gene transfer of an integrative and
671 conjugative element. *Proc Natl Acad Sci U S A* **113**:E3375-3383.
- 672 25. **Doucet-Populaire, F., P. Trieu-Cuot, I. Dosbaa, A. Andremont, and P. Courvalin.**
673 1991. Inducible transfer of conjugative transposon Tn1545 from *Enterococcus faecalis* to
674 *Listeria monocytogenes* in the digestive tracts of gnotobiotic mice. *Antimicrobial Agents*
675 *and Chemotherapy* **35**:185-187.
- 676 26. **Fernández-López, C., A. Bravo, S. Ruiz-Cruz, V. Solano-Collado, D. A. Garsin, F.**
677 **Lorenzo-Díaz, and M. Espinosa.** 2014. Mobilizable Rolling-Circle Replicating Plasmids
678 from Gram-Positive Bacteria: A Low-Cost Conjugative Transfer. *Microbiol Spectrum* **2**:8.
- 679 27. **Francia, M. V., D. B. Clewell, F. De La Cruz, and G. Moncalian.** 2013. Catalytic
680 domain of plasmid pAD1 relaxase TraX defines a group of relaxases related to restriction
681 endonucleases. *Proc Natl Acad Sci U S A* **110**:13606-13611.
- 682 28. **Franke, A. E., and D. B. Clewell.** 1981. Evidence for a chromosome-borne resistance
683 transposon (Tn916) in *Streptococcus faecalis* that is capable of "conjugal" transfer in the
684 absence of a conjugative plasmid. *J Bacteriol* **145**:494-502.
- 685 29. **Gawron-Burke, C., and D. B. Clewell.** 1982. A transposon in *Streptococcus faecalis* with
686 fertility properties. *Nature* **300**:281-284.
- 687 30. **Gibson, D. G., L. Young, R. Y. Chuang, J. C. Venter, C. A. Hutchison, 3rd, and H. O.**
688 **Smith.** 2009. Enzymatic assembly of DNA molecules up to several hundred kilobases. *Nat*
689 *Methods* **6**:343-345.

- 690 31. **Glaser, P., F. Kunst, M. Arnaud, M. P. Coudart, W. Gonzales, M. F. Hullo, M.**
691 **Ionescu, B. Lubochinsky, L. Marcelino, I. Moszer, and Et Al.** 1993. *Bacillus subtilis*
692 genome project: cloning and sequencing of the 97 kb region from 325 degrees to 333
693 degrees. *Mol Microbiol* **10**:371-384.
- 694 32. **Haima, P., S. Bron, and G. Venema.** 1987. The effect of restriction on shotgun cloning
695 and plasmid stability in *Bacillus subtilis* Marburg. *Mol Gen Genet* **209**:335-342.
- 696 33. **Haraldsen, J. D., and A. L. Sonenshein.** 2003. Efficient sporulation in *Clostridium*
697 *difficile* requires disruption of the sigmaK gene. *Mol Microbiol* **48**:811-821.
- 698 34. **Harwood, C. R., and S. M. Cutting.** 1990. *Molecular Biological Methods for Bacillus.*
699 John Wiley & Sons, Chichester.
- 700 35. **Henderson-Begg, S. K., A. P. Roberts, and L. M. Hall.** 2009. Diversity of putative
701 Tn5253-like elements in *Streptococcus pneumoniae*. *Int J Antimicrob Agents* **33**:364-367.
- 702 36. **Ireton, K., and A. D. Grossman.** 1992. Interactions among mutations that cause altered
703 timing of gene expression during sporulation in *Bacillus subtilis*. *J Bacteriol* **174**:3185-
704 3195.
- 705 37. **Jaacks, K. J., J. Healy, R. Losick, and A. D. Grossman.** 1989. Identification and
706 characterization of genes controlled by the sporulation-regulatory gene *spo0H* in *Bacillus*
707 *subtilis*. *J Bacteriol* **171**:4121-4129.
- 708 38. **Jaworski, D. D., and D. B. Clewell.** 1995. A functional origin of transfer (*oriT*) on the
709 conjugative transposon Tn916. *J Bacteriol* **177**:6644-6651.
- 710 39. **Johnson, C. M., and A. D. Grossman.** 2014. Identification of host genes that affect
711 acquisition of an integrative and conjugative element in *Bacillus subtilis*. *Mol Microbiol*
712 **93**:1284-1301.
- 713 40. **Johnson, C. M., and A. D. Grossman.** 2015. Integrative and Conjugative Elements
714 (ICEs): What They Do and How They Work. *Annu Rev Genet* **49**:577-601.
- 715 41. **Khan, S. A.** 2005. Plasmid rolling-circle replication: highlights of two decades of research.
716 *Plasmid* **53**:126-136.
- 717 42. **Khan, S. A.** 1997. Rolling-circle replication of bacterial plasmids. *Microbiol Mol Biol Rev*
718 **61**:442-455.
- 719 43. **Kramer, M. G., M. Espinosa, T. K. Misra, and S. A. Khan.** 1999. Characterization of a
720 single-strand origin, *ssoU*, required for broad host range replication of rolling-circle
721 plasmids. *Mol Microbiol* **33**:466-475.
- 722 44. **Kramer, M. G., S. A. Khan, and M. Espinosa.** 1997. Plasmid rolling circle replication:
723 identification of the RNA polymerase-directed primer RNA and requirement for DNA
724 polymerase I for lagging strand synthesis. *EMBO J* **16**:5784-5795.
- 725 45. **Lee, C. A., J. M. Auchtung, R. E. Monson, and A. D. Grossman.** 2007. Identification
726 and characterization of *int* (integrase), *xis* (excisionase) and chromosomal attachment sites
727 of the integrative and conjugative element ICEBsI of *Bacillus subtilis*. *Mol Microbiol*
728 **66**:1356-1369.
- 729 46. **Lee, C. A., A. Babic, and A. D. Grossman.** 2010. Autonomous plasmid-like replication of
730 a conjugative transposon. *Mol Microbiol* **75**:268-279.
- 731 47. **Lee, C. A., J. Thomas, and A. D. Grossman.** 2012. The *Bacillus subtilis* conjugative
732 transposon ICEBsI mobilizes plasmids lacking dedicated mobilization functions. *J*
733 *Bacteriol* **194**:3165-3172.
- 734 48. **Manganelli, R., L. Romano, S. Ricci, M. Zazzi, and G. Pozzi.** 1995. Dosage of Tn916
735 circular intermediates in *Enterococcus faecalis*. *Plasmid* **34**:48-57.

- 736 49. **Marra, D., and J. R. Scott.** 1999. Regulation of excision of the conjugative transposon
737 Tn916. *Mol Microbiol* **31**:609-621.
- 738 50. **Mcdonnell, G. E., and D. J. Mcconnell.** 1994. Overproduction, isolation, and DNA-
739 binding characteristics of Xre, the repressor protein from the *Bacillus subtilis* defective
740 prophage PBSX. *J Bacteriol* **176**:5831-5834.
- 741 51. **Minoia, M., M. Gaillard, F. Reinhard, M. Stojanov, V. Sentchilo, and J. R. Van Der**
742 **Meer.** 2008. Stochasticity and bistability in horizontal transfer control of a genomic island
743 in *Pseudomonas*. *Proc. Natl. Acad. Sci. U.S.A.* **105**:20792-20797.
- 744 52. **Mullany, P., R. Williams, G. C. Langridge, D. J. Turner, R. Whalan, C. Clayton, T.**
745 **Lawley, H. Hussain, K. Mccurrie, N. Morden, E. Allan, and A. P. Roberts.** 2012.
746 Behavior and target site selection of conjugative transposon Tn916 in two different strains
747 of toxigenic *Clostridium difficile*. *Appl Environ Microbiol* **78**:2147-2153.
- 748 53. **Naglich, J. G., and R. E. Andrews, Jr.** 1988. Tn916-dependent conjugal transfer of
749 pC194 and pUB110 from *Bacillus subtilis* into *Bacillus thuringiensis* subsp. *israelensis*.
750 *Plasmid* **20**:113-126.
- 751 54. **Norgren, M., and J. R. Scott.** 1991. The presence of conjugative transposon Tn916 in the
752 recipient strain does not impede transfer of a second copy of the element. *J Bacteriol*
753 **173**:319-324.
- 754 55. **Pabo, C. O., and R. T. Sauer.** 1984. Protein-DNA recognition. *Annu Rev Biochem*
755 **53**:293-321.
- 756 56. **Palmer, K. L., V. N. Kos, and M. S. Gilmore.** 2010. Horizontal gene transfer and the
757 genomics of enterococcal antibiotic resistance. *Curr Opin Microbiol* **13**:632-639.
- 758 57. **Paulsen, I. T., L. Banerjee, G. S. Myers, K. E. Nelson, R. Seshadri, T. D. Read, D. E.**
759 **Fouts, J. A. Eisen, S. R. Gill, J. F. Heidelberg, H. Tettelin, R. J. Dodson, L. Umayam,**
760 **L. Brinkac, M. Beanan, S. Daugherty, R. T. Deboy, S. Durkin, J. Kolonay, R.**
761 **Madupu, W. Nelson, J. Vamathevan, B. Tran, J. Upton, T. Hansen, J. Shetty, H.**
762 **Khouri, T. Utterback, D. Radune, K. A. Ketchum, B. A. Dougherty, and C. M. Fraser.**
763 2003. Role of mobile DNA in the evolution of vancomycin-resistant *Enterococcus faecalis*.
764 *Science* **299**:2071-2074.
- 765 58. **Perego, M., G. B. Spiegelman, and J. A. Hoch.** 1988. Structure of the gene for the
766 transition state regulator, *abrB*: regulator synthesis is controlled by the *spo0A* sporulation
767 gene in *Bacillus subtilis*. *Mol Microbiol* **2**:689-699.
- 768 59. **Ramsay, J. P., J. T. Sullivan, G. S. Stuart, I. L. Lamont, and C. W. Ronson.** 2006.
769 Excision and transfer of the *Mesorhizobium loti* R7A symbiosis island requires an integrase
770 IntS, a novel recombination directionality factor RdfS, and a putative relaxase RlxS. *Mol*
771 *Microbiol* **62**:723-734.
- 772 60. **Reinhard, F., R. Miyazaki, N. Pradervand, and J. R. Van Der Meer.** 2013. Cell
773 differentiation to "mating bodies" induced by an integrating and conjugative element in
774 free-living bacteria. *Curr Biol* **23**:255-259.
- 775 61. **Rice, L. B., L. L. Carias, S. Rudin, R. A. Hutton, and S. Marshall.** 2010. Multiple
776 copies of functional, Tet(M)-encoding Tn916-like elements in a clinical *Enterococcus*
777 *faecium* isolate. *Plasmid* **64**:150-155.
- 778 62. **Roberts, A. P., and P. Mullany.** 2009. A modular master on the move: the Tn916 family
779 of mobile genetic elements. *Trends Microbiol* **17**:251-258.

- 780 63. **Roberts, A. P., and P. Mullany.** 2011. Tn916-like genetic elements: a diverse group of
781 modular mobile elements conferring antibiotic resistance. *FEMS Microbiol Rev* **35**:856-
782 871.
- 783 64. **Rocco, J. M., and G. Churchward.** 2006. The integrase of the conjugative transposon
784 Tn916 directs strand- and sequence-specific cleavage of the origin of conjugal transfer,
785 *oriT*, by the endonuclease Orf20. *J Bacteriol* **188**:2207-2213.
- 786 65. **Scott, J. F.** 1993. Conjugative Transposons, p. 597-614. *In* A. L. Sonenshein, J. A. Hoch,
787 and R. Losick (ed.), *Bacillus subtilis and other Gram-positive bacteria: Biochemistry,*
788 *physiology, and molecular genetics.* American Society of Microbiology, Washington, D.C.
- 789 66. **Scott, J. R., P. A. Kirchman, and M. G. Caparon.** 1988. An intermediate in transposition
790 of the conjugative transposon Tn916. *Proc Natl Acad Sci U S A* **85**:4809-4813.
- 791 67. **Sebahia, M., B. W. Wren, P. Mullany, N. F. Fairweather, N. Minton, R. Stabler, N. R.**
792 **Thomson, A. P. Roberts, A. M. Cerdeno-Tarraga, H. Wang, M. T. Holden, A. Wright,**
793 **C. Churcher, M. A. Quail, S. Baker, N. Bason, K. Brooks, T. Chillingworth, A.**
794 **Cronin, P. Davis, L. Dowd, A. Fraser, T. Feltwell, Z. Hance, S. Holroyd, K. Jagels, S.**
795 **Moule, K. Mungall, C. Price, E. Rabinowitsch, S. Sharp, M. Simmonds, K. Stevens,**
796 **L. Unwin, S. Whithead, B. Dupuy, G. Dougan, B. Barrell, and J. Parkhill.** 2006. The
797 multidrug-resistant human pathogen *Clostridium difficile* has a highly mobile, mosaic
798 genome. *Nat Genet* **38**:779-786.
- 799 68. **Sentchilo, V., R. Ravatn, C. Werlen, A. J. B. Zehnder, and J. R. Van Der Meer.** 2003.
800 Unusual integrase gene expression on the *clc* genomic island in *Pseudomonas* sp. strain
801 B13. *J. Bacteriol.* **185**:4530-4538.
- 802 69. **Showsh, S. A., and R. E. Andrews, Jr.** 1999. Analysis of the requirement for a pUB110
803 mob region during Tn916-dependent mobilization. *Plasmid* **41**:179-186.
- 804 70. **Showsh, S. A., and R. E. Andrews, Jr.** 1992. Tetracycline enhances Tn916-mediated
805 conjugal transfer. *Plasmid* **28**:213-224.
- 806 71. **Sievers, F., A. Wilm, D. Dineen, T. J. Gibson, K. Karplus, W. Li, R. Lopez, H.**
807 **McWilliam, M. Remmert, J. Soding, J. D. Thompson, and D. G. Higgins.** 2011. Fast,
808 scalable generation of high-quality protein multiple sequence alignments using Clustal
809 Omega. *Mol Syst Biol* **7**:539.
- 810 72. **Smillie, C., M. P. Garcillan-Barcia, M. V. Francia, E. P. Rocha, and F. De La Cruz.**
811 2010. Mobility of plasmids. *Microbiol Mol Biol Rev* **74**:434-452.
- 812 73. **Smith, J. L., J. M. Goldberg, and A. D. Grossman.** 2014. Complete genome sequences
813 of *Bacillus subtilis* subsp. *subtilis* laboratory strains JH642 (AG174) and AG1839. *Genome*
814 *Announc* **2**.
- 815 74. **Smits, W. K., and A. D. Grossman.** 2010. The transcriptional regulator Rok binds A+T-
816 rich DNA and is involved in repression of a mobile genetic element in *Bacillus subtilis*.
817 *PLoS Genet* **6**:e1001207.
- 818 75. **Te Poele, E. M., H. Bolhuis, and L. Dijkhuizen.** 2008. Actinomycete integrative and
819 conjugative elements. *Antonie Van Leeuwenhoek* **94**:127-143.
- 820 76. **Thomas, J., C. A. Lee, and A. D. Grossman.** 2013. A conserved helicase processivity
821 factor is needed for conjugation and replication of an integrative and conjugative element.
822 *PLoS Genet* **9**:e103198.
- 823 77. **Wang, J., G. R. Wang, N. B. Shoemaker, and A. A. Salyers.** 2001. Production of two
824 proteins encoded by the *Bacteroides* mobilizable transposon NBU1 correlates with time-
825 dependent accumulation of the excised NBU1 circular form. *J Bacteriol* **183**:6335-6343.

- 826 78. **Washburn, M. P., D. Wolters, and J. R. Yates, 3rd.** 2001. Large-scale analysis of the
827 yeast proteome by multidimensional protein identification technology. *Nat Biotechnol*
828 **19**:242-247.
- 829 79. **Wilkins, B., and E. Lanka.** 1993. DNA Processing and Replication during Plasmid
830 Transfer between Gram-Negative Bacteria, p. 105-136. *In* D. B. Clewell (ed.), *Bacterial*
831 *Conjugation*. Springer US.
- 832 80. **Wood, H. E., M. T. Dawson, K. M. Devine, and D. J. Mcconnell.** 1990. Characterization
833 of PBSX, a defective prophage of *Bacillus subtilis*. *J Bacteriol* **172**:2667-2674.
- 834 81. **Wood, H. E., K. M. Devine, and D. J. Mcconnell.** 1990. Characterisation of a repressor
835 gene (*xre*) and a temperature-sensitive allele from the *Bacillus subtilis* prophage, PBSX.
836 *Gene* **96**:83-88.
- 837 82. **Wozniak, R. A., and M. K. Waldor.** 2010. Integrative and conjugative elements: mosaic
838 mobile genetic elements enabling dynamic lateral gene flow. *Nat Rev Microbiol* **8**:552-
839 563.
- 840 83. **Wright, L. D., C. M. Johnson, and A. D. Grossman.** 2015. Identification of a Single
841 Strand Origin of Replication in the Integrative and Conjugative Element ICEBsI of
842 *Bacillus subtilis*. *PLoS Genet* **11**:e1005556.
843
844
845

846 **Table 1. *Bacillus subtilis* strains used.**

Strain	Relevant genotype ^a (reference)
BS49	<i>metB5, hisA1, thr-5, att(yufKL)</i> ^b ::Tn916, <i>att(ykyB-ykuC)</i> ::Tn916 (10, 22, 33)
JMA222	ICEBsI ⁰ (2)
CMJ129	pHP13, <i>lacA</i> ::{(PrpsF-rpsF-ssb-mgfpmut2) tet} (83)
LDW173	<i>attI</i> ::Tn916 {same as <i>att(yufKL)</i> ::Tn916}
LDW631	<i>attI</i> ::Tn916 Δ <i>orf20-631</i> ; deletes most of <i>orf20</i> , leaves a functional <i>oriT</i>
LDW737	<i>amyE</i> ::{(attTn916) <i>spc</i> }
LDW815	pLW805 { <i>oriT(916)</i> , Pspank- <i>orf23-orf22-orf20, spc, lacI</i> }
LDW818	<i>attI</i> ::Tn916::pLW805 { <i>oriT(916)</i> , Pspank- <i>orf23-orf22-orf20, spc, lacI</i> }
LDW853	<i>attI</i> ::Tn916 <i>orf20-3UAA</i>
LDW872	pLW862 (pHP13ssiA <i>cat mls</i>), <i>lacA</i> ::{PrpsF-rpsF-ssb-mgfpmut2, tet}
LDW878	pLW868 (pHP13sso916 <i>cat mls</i>), <i>lacA</i> ::{PrpsF-rpsF-ssb-mgfpmut2, tet}
LDW879	pLW859 { <i>oriT(916)</i> , Pspank- <i>orf23-orf22-orf20-his6, spc, lacI</i> }
LDW894	pLW890 (pHP13sso916R <i>cat mls</i>), <i>lacA</i> ::{PrpsF-rpsF-ssb-mgfpmut2, tet}
LDW929	<i>attI</i> ::Tn916 Δ <i>orf20-631</i> , <i>lacA</i> ::{ <i>mls</i> , Pspank(hy)- <i>orf20-myc</i> , pLW920 <i>spc</i> }; pLW920 is integrated into <i>orf20</i> to generate <i>orf20-myc</i>
LDW930	<i>attI</i> ::Tn916 Δ <i>orf20-631</i> , <i>lacA</i> ::{ <i>mls</i> , Pspank(hy)- <i>orf20</i> Δ <i>hth-myc</i> , pLW920 <i>spc</i> }; pLW920 is integrated into <i>orf20</i> Δ <i>hth</i> to generate <i>orf20</i> Δ <i>hth-myc</i>
LDW931	<i>attI</i> ::Tn916 <i>orf20-3UAA</i> , <i>lacA</i> ::{ <i>mls</i> , Pspank(hy)- <i>orf20-myc</i> , pLW920 <i>spc</i> }
LDW932	<i>attI</i> ::Tn916 <i>orf20-3UAA</i> , <i>lacA</i> ::{ <i>mls</i> (Pspank(hy)- <i>orf20</i> Δ <i>hth-myc</i> , pLW920 <i>spc</i>)

847

848 ^a All strains except BS49 are derived from JH642 and contain the *trpC2 pheA1* alleles (58,
849 73). Strains do not contain Tn916 unless Tn916 is specifically indicated.

850 ^b *attI* is the same as *att(yufKL)* and is located between *yufK* and *yufL*.

851

852

853 **Table 2. Mass spectrometry of affinity-purified Orf20-his shows that the HelP homologues**
854 **are associated with the relaxase.**

855

Protein	% Sequence coverage ^a	# Peptides ^b	MW (kDa) ^c
Orf20 relaxase	51.5	84	46.8
Orf22 HelP	67.2	33	14.1
Orf23 HelP	69.6	18	11.8

856

857 ^a Percentage of the protein sequence detected by mass spectrometry. Amino acid sequences were
858 based on *Tn916* genes (GenBank U09422.1) except Orf20, which was based on the re-annotated
859 gene starting at CUG and containing the N-terminal helix-turn-helix region (Fig. 3B).

860

861 ^b Number of total peptides detected.

862

863 ^c Predicted molecular weight in kilodaltons.

864

865

866

867 **Table 3. Complementation of the Tn916 replication defects of relaxase mutants $\Delta orf20$ and**
 868 ***orf20-3UAA*.**

869

Line	Tn916 genotype	Pspank(hy) ^a	Circles per excision ^b
1	wild type	---	6.05 (± 0.43)
2	$\Delta orf20$	---	0.43 (± 0.12)
3	<i>orf20-3UAA</i>	---	0.61 (± 0.26)
4	$\Delta orf20$	<i>orf20-myc</i>	8.03 (± 2.94)
5	<i>orf20-3UAA</i>	<i>orf20-myc</i>	6.98 (± 1.60)
6	$\Delta orf20$	<i>orf20Δhth-myc</i>	0.55 (± 0.08)
7	<i>orf20-3UAA</i>	<i>orf20Δhth-myc</i>	0.46 (± 0.17)

870

871 ^a*orf20* complementation alleles were expressed in trans at the *lacA* locus and driven by promoter
 872 Pspank(hy).

873

874 ^bCircles per excision were quantified by qPCR by measuring the amount of the circular junction
 875 *attTn916* relative to the vacant chromosome site *attI* (Fig. 1A). Data are averages from 3
 876 independent experiments (\pm standard deviation). Strains were LDW173, LDW631, LDW853,
 877 LDW929, LDW931, LDW930 and LDW932 (lines 1-7).

878

879

880 **Table 4. *sso916* is conserved in other Tn916-like ICEs.**

ICE ^a	Organism ^b
Tn6009	<i>Klebsiella pneumoniae</i> 41
ICESpnH034800032	<i>Streptococcus pneumoniae</i> H034800032
CTn6009	<i>Streptococcus cristatus</i>
ICESpn9409	<i>S. pneumoniae</i> 9409
ICESpn11928	<i>S. pneumoniae</i> 11928
ICESpnMalM6	<i>S. pneumoniae</i> Mal M6
ICESpn11930-2	<i>S. pneumoniae</i> 11930
ICESpn23771	<i>S. pneumoniae</i> 23771
ICESpn11876	<i>S. pneumoniae</i> 11876
ICESpn11930	<i>S. pneumoniae</i> 11930
ICESsu(BM407)1	<i>Streptococcus suis</i> BM407
ICESsu(BM407)2	<i>S. suis</i> BM407
ICESp23FST81	<i>S. pneumoniae</i> ATCC 700669
ICESsu(SC84)	<i>S. suis</i> SC84
Tn5397	<i>Clostridium difficile</i> 630
Tn1545	<i>S. pneumoniae</i> BM4200

881

882 ^aICEs with regions similar to the intergenic sequence containing *sso916* were identified using
883 WU-BLAST 2.0 and searching the ICEberg v1.0 database of ICE nucleotide sequences (6). The
884 search identified *sso916* in Tn5251, which is essentially identical to Tn916 (>95% identity at the
885 nucleotide level) and is not included in the table. ICESpnH034800032 and CTn6002 are listed
886 separately in ICEberg and were identified in different organisms, but are essentially identical
887 elements (>95% identity at the nucleotide level). Conservation of each putative *sso* with *sso916*
888 is 100% except for Tn5397 and Tn1545, which have 94% and 96% identity, respectively.

889

890 ^b Each ICE was initially identified in the indicated species and strain.

891

892 **Figure legends**

893 **Figure 1. Genetic map of Tn916 and schematic for detecting excision products.** The ends
 894 of Tn916 are indicated by black rectangles. **(A)** Map of Tn916. Rectangular gray arrows
 895 represent the genes in Tn916 and the direction of transcription. *orf23* and *orf22* encode
 896 homologues of the helicase processivity factor (HelP from ICEBs1) and *orf20* encodes the
 897 relaxase needed for DNA transfer and replication. All other gene names (numbers) are indicated
 898 above the corresponding gene. *oriT(916)* (38) and *ss0916* are indicated with thick black lines.
 899 **(B)** Cartoon of the qPCR strategy to measure Tn916 replication. Excision of Tn916 from the
 900 chromosome of strain LDW173 produces 1) circular Tn916 containing site *attTn916* and 2)
 901 vacated chromosome site *attI*. The products are detected via qPCR using primers b and c
 902 (primers oLW526 and oLW527), or a and d (primers oLW542 and oLW543), respectively,
 903 which are represented as small black arrows.

904

905 **Figure 2. Products generated following excision of Tn916 from the chromosome.** Cells
 906 containing Tn916 (strain LDW173, triangles) or Tn916 Δ *orf20* (LDW631, circles) were grown in
 907 the presence (filled symbols) or absence (open symbols) of 2.5 μ g/ml tetracycline. Quantitative
 908 PCR data (black lines, left axes) and growth phase as determined by OD₆₀₀ (gray lines, right
 909 axes) are shown. Strain LDW737 contains one copy of each qPCR amplicon (*attTn916*; *attI*;
 910 and *mrpG*) and was used to generate standard curves for qPCR (see Materials and Methods). **(A)**
 911 Excision of Tn916. The vacated chromosomal site *attI* was amplified by qPCR, and *attI* signal
 912 was normalized to the signal of an unrelated chromosomal locus, *mrpG*. **(B)** The average copy
 913 number of circular Tn916 per host chromosome. The *attTn916* junction present in the circular
 914 (excised) form of Tn916 was amplified by qPCR, and the qPCR signal was normalized to that of
 915 chromosomal gene *mrpG*. **(C)** Tn916 circles per excision event. Circular Tn916 (*attITn916*) was
 916 amplified by qPCR, and the *attITn916* signal was normalized to that of the *attI* site formed from
 917 excision. Data are means \pm standard deviation of ≥ 4 independent experiments.

918

919

920 **Figure 3. The relaxase encoded by *orf20* contains a conserved N-terminal helix-turn-**
 921 **helix region. (A)** The revised amino acid sequence of the Tn916 relaxase (Orf20). The
 922 methionine previously thought to be the start of the protein is indicated in bold (M). Peptides
 923 identified by mass spectrometry were mapped to the amino acid sequence of Orf20 and are
 924 underlined. The bold underline indicates peptides that overlapped the junction between the N
 925 terminal region and what was previously thought to be the initiating methionine. **(B-D)** Maps of
 926 *orf20* and *orf20* overexpression alleles used here. Gray arrows correspond to the *orf20* coding
 927 sequence and the direction of transcription. The dark gray rectangles represent the conserved
 928 XRE-like helix-turn-helix (HTH) and relaxase regions in *orf20* as determined using the NCBI
 929 Conserved Domain Database (see Materials and Methods). The black rectangles represent the
 930 putative ribosome binding site (RBS) that is present in Tn916 and preserved in the myc-tagged
 931 alleles. **(B)** *orf20* in Tn916 and upstream sequence. The hatched black arrow represents the C
 932 terminus of *orf21*. The CUG codon and previously proposed AUG start codons are indicated.
 933 The relative location of the UAA nonsense mutation in *orf20-3UAA* is marked with an asterisk.
 934 **(C-D)** Myc-tagged *orf20* alleles with **(C; WT *orf20*)** or without **(D; *orf20* Δ *hth*)** the N terminal
 935 helix-turn-helix region. The C-terminal myc tags are not shown. *orf20*-myc alleles were driven
 936 by promoter Pspank(hy) (black arrow). **(C)** WT*orf20*-myc contains the entire coding sequence as
 937 depicted in (A) and non-coding DNA upstream of the CUG start. **(D)** *orf20* Δ *hth*-myc contains the
 938 *orf20* coding sequence starting at the previously proposed AUG start codon as depicted in (A)
 939 and non-coding DNA upstream of the CUG start.

940

941 **Figure 4. Alignment of several relaxase homologues.** The amino acid sequences of the
 942 relaxases from Tn916, Tn5253, CTn7, CTnI and ICEBsI were aligned with the Clustal Omega
 943 algorithm (<http://www.ebi.ac.uk/Tools/msa/clustalo/>) (71). Black-shaded residues are identical in
 944 all five relaxases, and gray-shaded residues are similar in all relaxases. The helix-turn-helix
 945 region present in four of the five relaxases is boxed. Previously proposed N-terminal methionines
 946 in *orf20* of Tn916 and *orf26* of CTnI are bolded and boxed. The output alignment was shaded
 947 using BoxShade (http://www.ch.embnet.org/software/BOX_form.html). The order of sequences
 948 (Tn916 Orf20 to ICEBsI NicK) reflects the order of the original input queries; closely related
 949 sequences were not computationally grouped in the final alignment.

950

951

952 **Figure 5. Ssb-GFP to visualize ssDNA and single strand origin activity.** All cells contain
 953 ssDNA-binding protein Ssb fused to GFP. Phase contrast (top panels) and GFP fluorescence
 954 (bottom panels) are shown. **(A)** No plasmid, strain CMJ118. In cells without a plasmid, Ssb-GFP
 955 forms small foci at the replication forks (white arrow) (5). **(B)** pHP13, strain CMJ129. Ssb-GFP
 956 forms large foci (white arrowhead) in cells containing pHP13, which does not encode a
 957 functional *ssO* and accumulates ssDNA (83). **(C)** pHP13*ssiA*, strain LDW872. The primosome
 958 binding site *ssiA* from pAM β , which can function as an *ssO* in rolling circle replicating plasmids
 959 and reduce ssDNA (11), was cloned into pHP13 to make pHP13*ssiA* (pLW862). Cells
 960 containing pHP13*ssiA* had small foci of Ssb-GFP (white arrow) **(D)** pHP13*ssO916*, strain
 961 LDW878. Cells containing pHP13 with the *ssO* from Tn916 (pLW868) did not accumulate large
 962 Ssb-GFP foci (white arrow), indicating reduced ssDNA. **(E)** pHP13*ssO916R*, strain LDW894.
 963 Cells containing pHP13 with *ssO916* cloned in the reverse orientation (pLW890) had large Ssb-
 964 GFP foci (white arrowhead), indicating accumulation of ssDNA. Data are representative images
 965 from ≥ 3 independent experiments.

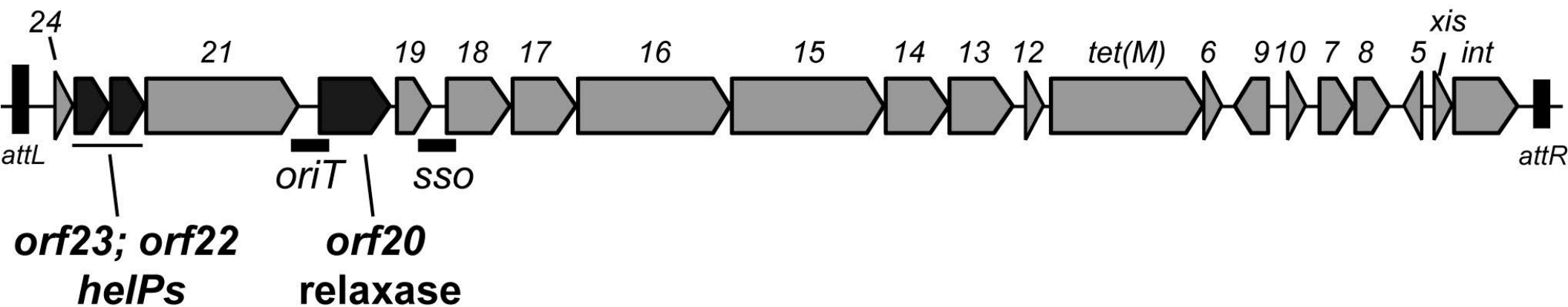
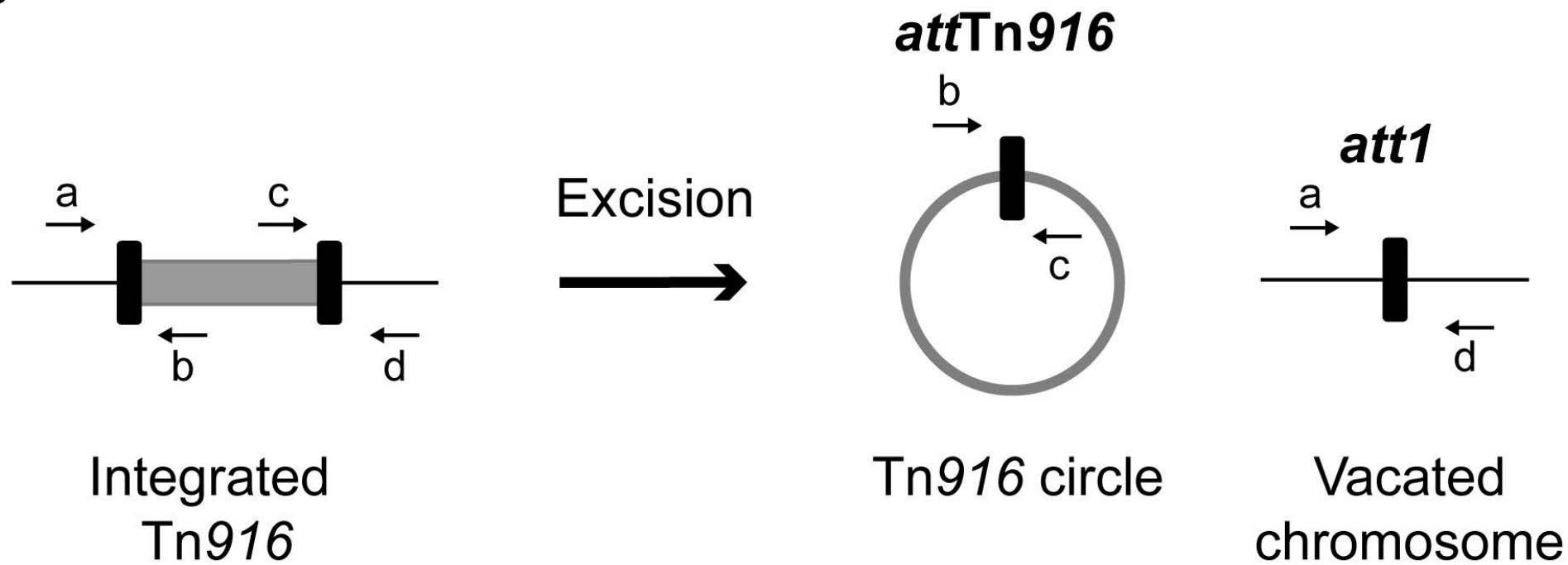
966

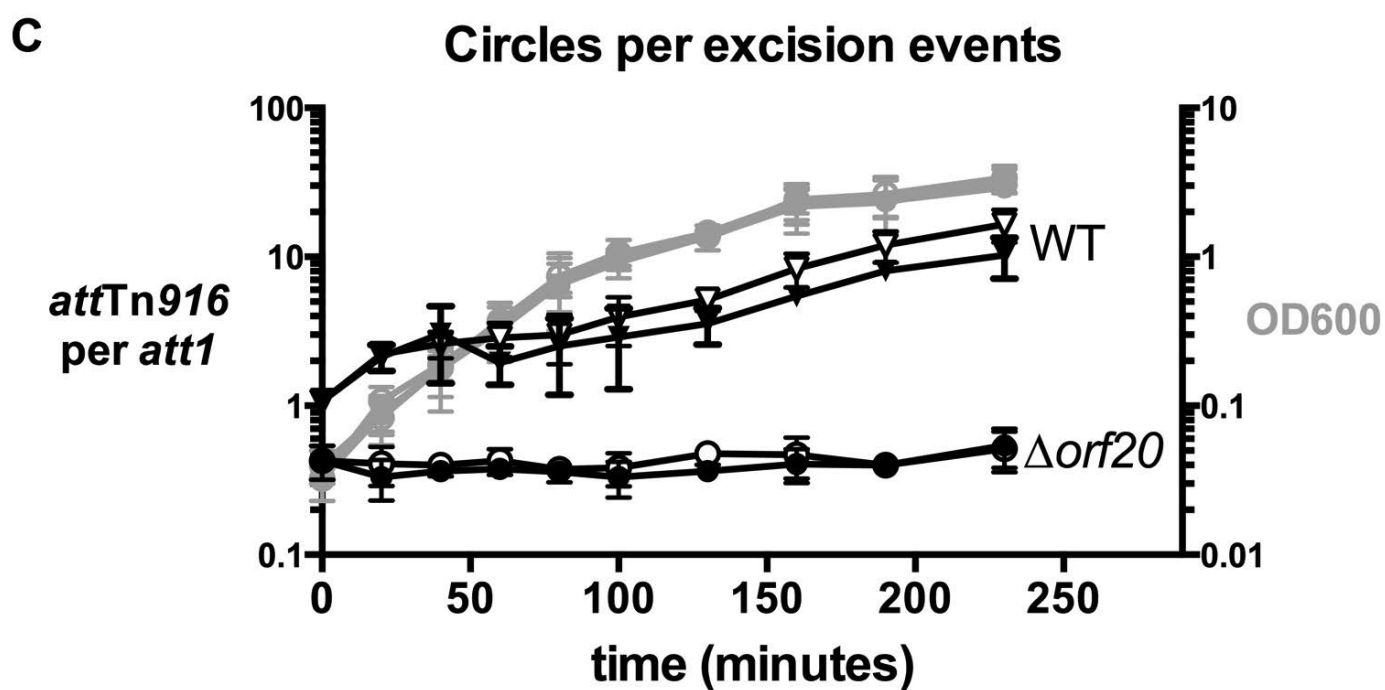
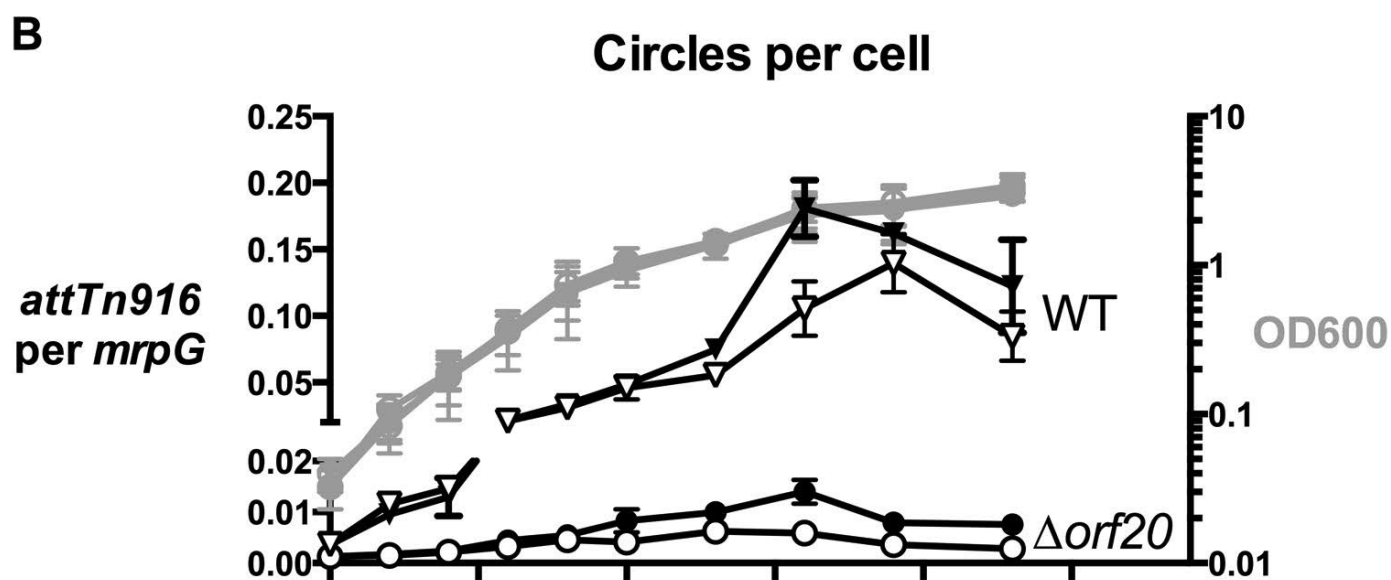
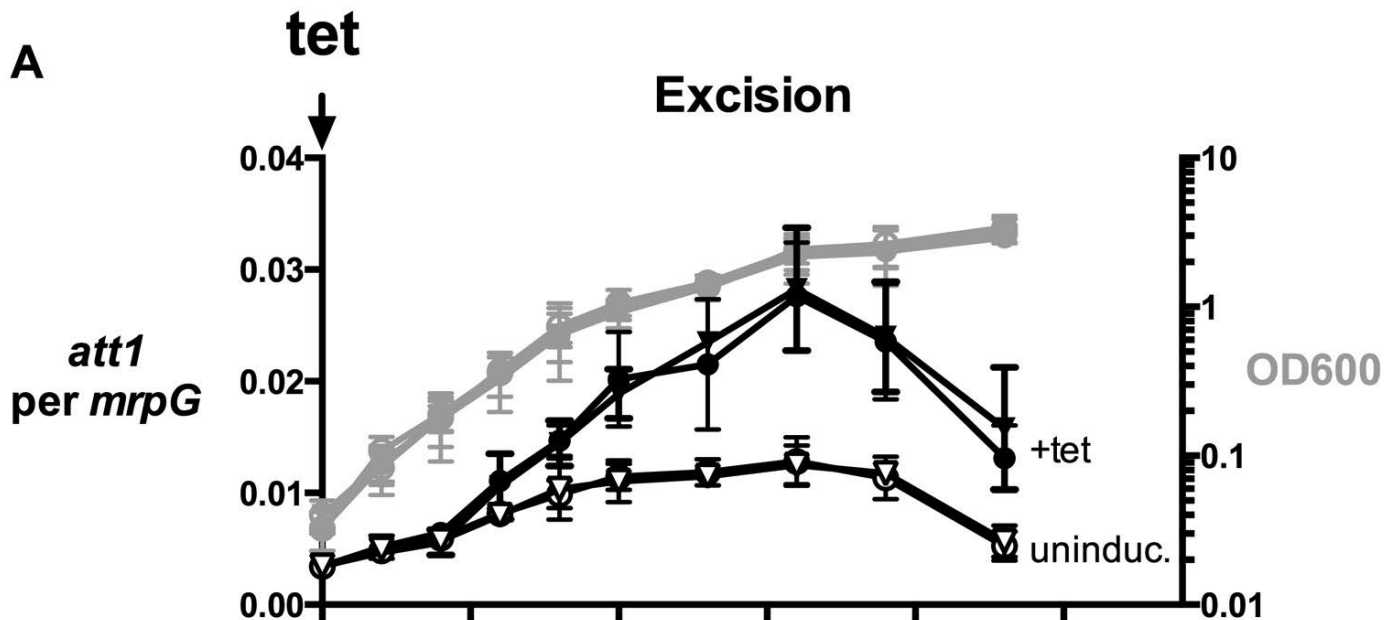
967

968 **Figure 6. *ssO916* reduces the amount of Ssb-GFP bound to plasmid DNA.** Plasmid DNA
 969 associated with Ssb-GFP. Ssb-GFP was immunoprecipitated following crosslinking with
 970 formaldehyde. The amount of plasmid DNA that was co-immunoprecipitated (with Ssb-GFP)
 971 was amplified with qPCR using primers to the *cat* gene in pHP13. The amounts of PCR
 972 products were normalized to the amount of plasmid DNA in total lysates, essentially as described
 973 (83). Data are means \pm standard deviation of biological triplicates.

974

975

A**B**



A Mass spectrometry peptide coverage of Orf20 relaxase

MNEQTLWLQHLKEKRLAYGLSQNRLAVATGITRQYLSDIETGKVKPSEDLQOQSLWEALERFNPDAPL
EMLEFDYVRIRFPPTTDVQQVVENILQLKLSYFLHEDYGFYSYSEHYALGDI FVLC SHELDKGVLEVEL
KGRGCRQFESYLLAQQRSWYEFFMDVLVAGGVMKRLDLAINDKTGILNIPVLTEKCQQEECISVFR
SFKSYRSGELVRKEEKECMGNTLYIGSLQSEVYFCIYEKDYEQYKKNDIPIEDAENVKNRFEIRLKN
ERAYYAVRDLLVYDNPEHTAFKIINRYIRFVDKDDSKPRSDWKLNEEWAWFIGNNRERLKLTTKPE
PYSFQRTLNLWLSHQVAPTLKVAIKLDEINQTQVVKDILDHAKLTDHRHKQILKQQSVKEQDVITTKK

B *orf20* re-annotated



Helix-turn-helix

Tn916_Orf20 1 ----MNEQTWLQHL**KEKRLAYGLSQNRLAVATGITROYLSDIETGKVKPSEDLQOQSLWEALE**RFNPDAP
Tn5253_Orf20 1 MEGFLLNEQTWLQHL**KEKRLAYGLSQNRLAVATGITROYLSDIETGKVKPSEDLQOQSLWEALE**RFNPDAP
CTn7_Orf27 1 ---MVLNEEQWIKEL**REKRIAYGISQGR LAVASGITREYLNKIESGKMKPSKELLHTLHKELA**RFNPETP
CTn1_Orf26 1 ----MNEKDFLTAL**KEKRCDYGV SOTRLAIMAGISREHLSRIEAGKVTLTEDMKHKLLEAVE**KFNPDNP
ICEBs1_Nick 1 -----MDELKOPPHA-NRGVVIVKEKNEAVES

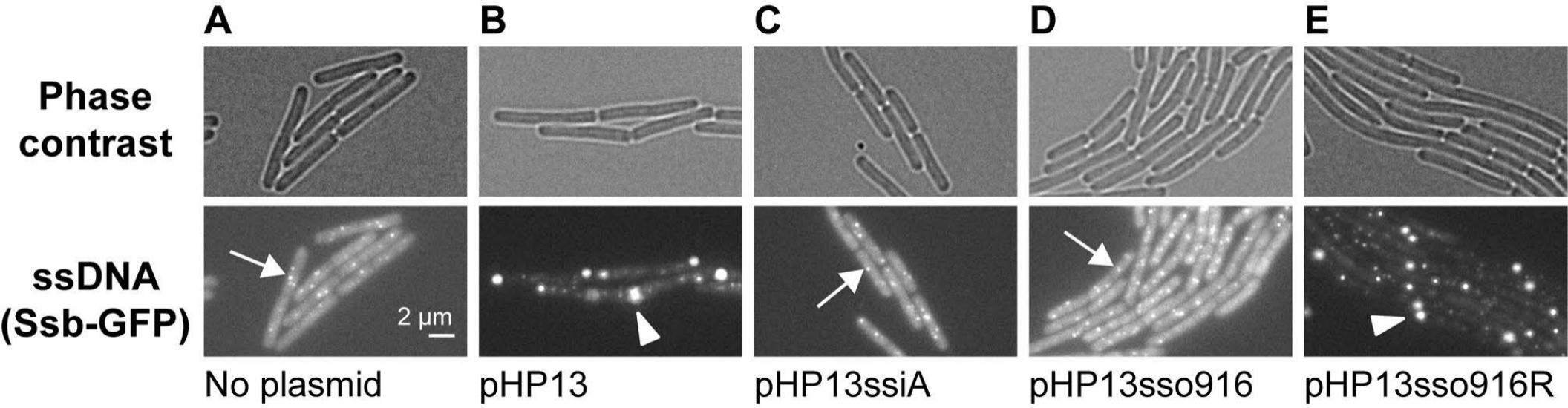
Tn916_Orf20 66 L**EM**LF**DY**VRIR**FPTT**DV**Q**Q**V**VENI**LQ**L**K**LSY**FL**HEDY**GF**YS**Y**SEHY**AL**GD**I**F**V**LC**S**HELD**K**G**V**L**V**EL**K**GR
Tn5253_Orf20 71 L**EM**LF**DY**VRIR**FPTT**DV**Q**Q**V**VENI**LQ**L**K**LSY**FL**HEDY**GF**YS**Y**SEHY**AL**GD**I**F**V**LC**S**HELD**K**G**V**L**V**EL**K**GR
CTn7_Orf27 68 L**T**M**L**FD**Y**V**K**IR**FPTL**D**I**Q**H**I**I**KD**I**L**K**L**N**I**N**Y**M**L**H**EDY**GH**YS**Y**TEHY**S**LGD**I**F**I**Y**T**S**A**DEEK**G**V**L**LE**L**K**G**R
CTn1_Orf26 66 M**F**LL**F**D**Y**VRIR**FPTT**D**I**Q**H**I**I**KD**I**L**K**L**N**I**N**Y**M**L**H**EDY**GH**Y**K**Y**T**E**H**Y**H**I**G**E**V**F**V**Y**V**S**Q**DEEK**G**V**L**LE**L**K**G**K
ICEBs1_Nick 28 L**V**S**M**V**D**Y**I**R**V**S**F**K**T**H**D**V**D**R**I**I**E**E**V**L**H**L**S**K**D**F**M**T**E**K**Q**S**G**F**Y**G**Y**V**G**T**Y**E**L**D**Y**I**K**V**F**Y**S**A**P**D**D**R**G**V**L**I**E**M**S**G**Q**

Tn916_Orf20 136 G**C**R**Q**F**E**S**Y**L**L**A**Q****Q**R**S**W**Y**E**F**F**M**D**V**L**V**A**G**G**V**M**K**R**L**D**L**A**I**N**D**K**T**G**I**L**N**I**P**V**L**T**E**K**C**Q**Q**E**E**C**I**S**V**F**R**S**F**K**S**Y**R**S
Tn5253_Orf20 141 G**C**R**Q**F**E**S**Y**L**L**A**Q****Q**R**S**W**Y**E**F**F**M**D**V**L**V**A**G**G**V**M**K**R**L**D**L**A**I**N**D**K**T**G**I**L**N**I**P**V**L**T**E**K**C**Q**Q**E**E**C**I**S**V**F**R**S**F**K**S**Y**R**S
CTn7_Orf27 138 G**C**R**Q**F**E**S**Y**L**L**A**Q****Q**R**S**W**Y**D**F**L**M**D**A**L**V**D**G**G**V**M**K**R**I**D**L**A**I**N**D**H**T**G**I**L**D**I**P**E**L**A**E**K**C**R**K**R**E**Y**I**G**K**S**R**S**Y**K**F**Y**Q**S
CTn1_Orf26 136 G**C**R**Q**F**E**S**Y**L**L**A**Q****E**R**S**W**Y**D**F**F**M**D**A**L**V**E**G**G**V**M**K**R**I**D**L**A**I**N**D**R**T**G**L**L**D**I**P**E**L**I**Q**K**E**N**E**E**C**I**S**K**F**R**S**F**K**N**Y**G**S**
ICEBs1_Nick 98 G**C**R**Q**F**E**S**F**L**E**C**R**K**K**T**W**Y**D**F**F**Q**D**C**M**Q**Q**G**G**S**F**T**R**F**D**L**A**I**D**D**K**K**T**Y**F**S**I**P**E**L**L**K**K**A**Q**K**G**E**C**I**S**R**F**R**K**S**D**F**N**G**S**

Tn916_Orf20 206 G**E**L**V**R**K**E**E**--**K**E**C**M**G**N**T**L**Y**I**G**S**L**O**S**E**V**Y**F**C**I**Y**E**K**D**Y**E**Q**Y**K**K**N**D**I**P**I**E**D**A**E**V**K**N**R**F**E**I**R**L**K**N**E**R**A**Y**Y**A**V**R**D
Tn5253_Orf20 211 G**E**L**V**R**K**E**E**--**K**E**C**M**G**N**T**L**Y**I**G**S**L**O**S**E**V**Y**F**C**I**Y**E**K**D**Y**E**Q**Y**K**K**N**D**I**P**I**E**D**A**E**V**K**N**R**F**E**I**R**L**K**N**E**R**A**Y**Y**A**V**R**D
CTn7_Orf27 208 G**E**L**I**K**H**R**E**D--**E**Y**M**G**R**T**L**Y**L**G**S**L**K**S**D**V**Y**F**C**I**Y**E**K**D**Y**E**Q**Y**V**K**L**G**I**P**L**E**A**D**I**N**R**F**E**I**R**L**R**N**E**R**A**Y**Y**A**V**R**D**
CTn1_Orf26 206 G**E**L**V**K**H**N**E**T**D**K**G**M**G**H**T**L**Y**I**G**S**F**S**S**E**V**Y**F**C**C**Y**E**K**N**Y**E**Q**Y**A**K**L**G**I**P**I**E**E**V**P**I**K**N**R**F**E**I**R**L**K**N**E**R**A**Y**Y**A**V**R**E
ICEBs1_Nick 168 F**D**L**S**D----**G**I**T**G**G**T**I**Y**F**G**S**K**K**S**E**A**Y**L**C**F**Y**E**K**N**Y**E**Q**A**E**K**Y**N**I**P**L**E**E**L**G**D**W**N**R**Y**E**L**R**L**K**N**E**R**A**Q**V**A**I**D**A**

Tn916_Orf20 274 L**L**V**Y**D**N**P**E**H**T**A**F**K**I**I**N**R**Y**I**R**F**V**D**K**D**S**K**P**R**S**D**W**K**L**N**E**E**W**A**F**I**G**N**N**R**E**R**L**K**L**T**T**K**P**E**P**Y**S**F**Q**R**T**L**N**W**L**S**H**
Tn5253_Orf20 279 L**L**V**Y**D**N**P**E**H**T**A**F**K**I**I**N**R**Y**I**R**F**V**D**K**D**S**K**P**R**S**D**W**K**L**N**E**E**W**A**F**I**G**N**N**R**E**R**L**K**L**T**T**K**P**E**P**Y**S**F**Q**R**T**L**N**W**L**S**H**
CTn7_Orf27 276 L**L**T**Y**Y**D**A**E**Q**T**A**F**S**V**I**N**Q**Y**V**R**F**V**D**E**E**P**D**K**R**K**N**D**W**K**L**N**D**R**W**A**F**I**G**D**N**R**Q**S**L**K**L**T**T**K**P**E**P**Y**T**L**D**R**T**L**R**W**V**Q**R
CTn1_Orf26 276 L**L**T**N**Y**D**A**E**L**T**A**F**S**I**I**N**Q**Y**I**R**F**A**D**K**E**P**D**K**R**K**S**D**W**K**T**N**A**R**W**S**F**I**G**E**G**R**P**P**I**K**L**T**T**K**P**E**P**F**T**M**E**R**T**M**K**W**L**Q**R
ICEBs1_Nick 233 L**L**K**T**K**D**L**T**L**I**A**M**Q**I**I**N**N**Y**V**R**F**V**D**A**D**E**N**I**T**R**E**H**W**K**T**S**L**F**W**S**D**F**I**G**D**V**-**G**R**L**P**L**Y**V**K**P**Q**K**D**F**Y**Q**K**S**R**N**W**L**R**N**

Tn916_Orf20 344 Q**V**A**P**T**L**K**V**A**I**K**L**D**E**I**N**Q**T**Q**V**V**K**D**I**L**D**H**A**K**L**T**D**R**H**K**Q**I**L**K**Q**S**V**K**E**Q**D**V**I**T**T**K**K**
Tn5253_Orf20 349 Q**V**A**P**T**L**K**V**A**I**K**L**D**E**I**N**Q**T**Q**V**V**K**D**I**L**D**H**A**K**L**T**D**R**H**K**Q**I**L**K**Q**S**V**K**E**Q**D**V**I**T**T**K**K**
CTn7_Orf27 346 Q**V**A**P**T**L**K**M**L**K**K**I**D**K**G**N**G**T**D**Y**M**E**T**I**E**Q**Q**A**K**L**T**E**K**H**E**M**I**I**K**Q**Q**T**T**P**A**K**D**L**V**K**S--
CTn1_Orf26 346 Q**V**A**P**T**L**K**M**M**K**K**I**D**K**G**N**G**T**D**Y**M**E**T**I**E**Q**Q**A**K**L**T**E**K**H**E**M**I**I**K**Q**Q**T**T**P**A**K**D**L**V**E**S--
ICEBs1_Nick 302 S**C**A**P**T**M**K**M**V**L**E**A**D**E**H**L**G**K**T**D**L**S**D**M**I**A**E**A**E**L**A**D**K**H**K**M**L**D**V**Y**M**A**D**V**A**D**M**V**V---



ssDNA

% of input
amount of plasmid
DNA bound to Ssb

